Simulating interaction between sloped seabeds and preload capacity of jack-ups

Thesis Report

Simon Speetjens

Simulating interaction between sloped seabeds and preload capacity of jack-ups

Thesis Report

by

Simon Speetjens

Thesis Committee:	Dr. Ir. E. Kementzetzidis	TU Delft, chairman
	Dr. Ir. Colomés Gene	TU Delft, supervisor
	Ir. T. Blankenstein	GustoMSC
Faculty:	Offshore and Dredging Engineering, Delft	

Acknowledgements

This thesis was written as a conclusion to the master Offshore Engineering and Dredging with specialisation on Bottom Founded Structures at the Delft University of Technology. This thesis is written in cooperation with GustoMSC.

I would like to thank my whole committee for helping me through this thesis.
Firstly I would like to thank my daily supervisor at the company Tobias Blankenstein, with whom I have had numerous meetings with discussing progress and results.
Secondly I would like to thank my chair committee Vagelis Kementzetzidis for all his input on the geotechnical aspects of this project and helping me comprehend this previously unknown domain.
Thirdly, I would like to thank Oriol Colomes Gene for his input on the structural modelling aspects of this thesis during our progress meeting.
Lastly I would also like to thank my colleague Raluca Toma for helping me get along with the Plaxis program and being readily available for quick consults when I would get stuck in the soil model.

I would also like to thank Silke Bodewes for calming me down when the stress of the thesis would get to me and keeping me from working (most) weekends.
Also I would like to thank my mom and siblings for supporting me and keeping my head up when we went on vacation to Italy.

Simon Speetjens
Rotterdam, August 2024

Abstract

In the current energy market, where increasing demand for renewable energy is met with larger turbines which require larger installation vessels, understanding operational limits of such vessels becomes invaluable. For the installation of wind turbine generators at great heights, a stable working platform is offered by jack-up (JU) vessels, which use legs to elevate the hull and thus crane of the vessel above the waves. The operation taken into consideration is the preloading process where load is increased on the legs to ensure enough foundation capacity for later operations such as lifting of wind turbine generators. Traditionally, vessels have only been positioned above flat seabeds, but with the increased demand in the wind sector, unfavorable locations with sloped seabeds also need to be considered.

In order to capture global behaviour of a JU on a sloped seabed, two modelling methods are combined to create a framework; soil-structure interaction and structural finite element model. This framework implements a sub structuring approach by cutting and simulating a single leg on a sloped seabed using soil-structure interaction modelling. The results of the first method are foundation stiffness values and reaction loads during preloading of the JU while the second method takes those results as input to calculate internal loads of the JU.

The results show that the proposed framework is able to fulfill the task of combining two models and obtain meaningful results that can inform the JU during preloading phase. Then with this framework, the results show that sloped seabed induces an extra set of moments and lateral loads due to the asymmetric seabed causing an eccentric reaction load. These moments are then redistributed through the JU to other legs and their footings.

These results imply that for a JU on a sloped seabed, a framework combining geotechnical and structural domains can be applied to show the increased load due to the sloped seabed. Additional to the results, a sensitivity study is implemented for a variation of soil type and soil-structure geometry, the latter providing a more realistic seabed slope and larger reaction loads.

Contents

List of Figures

List of Tables

Nomenclature

Abbreviations

Abbreviation	Definition
ALE	Arbitrary Lagrangian-Eulerian
CEL	Coupled Eulerian Lagrangian
DNV	Der Norske Veritas
DOF	Degree Of Freedom
FE	Finite Element
HS	Hardening Soil
ISO	International Organisation for Standards
JU	Jack-Up
LDFE	Large Deformation Finite Element
LE	Linear Elastic
LP	Leg Pair
MC	Mohr-Coulomb
ME	Macro Element
PDE	Partial Differential Equation
RD	Relative Density
RD25	Relative Density of 25%
RD50	Relative Density of 50%
RD80	Relative Density of 80%
RPD	Rack Phase Difference
SSFE	Smal Strain Finite Element
WTIV	Wind Turbine Installation Vessel

1 Introduction

Jack-up (JU) vessels are essential to the offshore industry for a wide range of tasks, from drilling in shallow waters to supporting intricate construction projects such as installation of offshore wind turbines. Since these adaptable structures are essential to offshore operations, it is critical to have a thorough grasp of their behavior. One main aspect of a JU is the need for preloading before any lifting operation can be done, where preloading refers to the vertical loading of a leg past the expected operational leg loads in order to negate further settlement of the leg during operation. The problem arises, as the wind market keeps expanding and more vessels are used in various environments, the need for determining the limits of operations for these vessels keeps growing. Current industry standards are mostly based on flat seabeds but since sloped seabeds can have substantial effect on structural integrity of JU's, thorough understanding of the JU footing and sloped seabeds is required.

Classically describing the jack-up structure behaviour (structural) and seabed interaction effects (geotechnical) are done separately, but in this report these two fields are combined in order to give insight on the problem described. Using the identified problem as a starting point, this report explores a methodical approach to closing the knowledge gap by expanding upon the identified problem and formulating a research question in order to give a solution to the problem. This research question is then solved by formulating a methodology which delivers results from which conclusions can be made in order to answer the research questions.

1.1. Problem definition

Jack-up vessels are able to work in various conditions but there is very little known about preloading operations occurring on sloped seabeds. This research divides the problem into two domains as the preloading process can be seen as a combination of a geotechnical and structural problem.
Where firstly soil-structure interaction belongs to the geotechnical domain, with selection of soil constitutive model and soil parameters, virtual soil testing, implementation of a soil continuum and translation of load-displacement to uniaxial stiffness values.
Secondly the JU during preloading must be modelled, in order to describe load distribution during preloading operation of a JU on a sloped seabed.
The problem of a sloped seabed occurs when a vessel performs a jacking operation where a seabed slope seems to be present, where jacking refers to lifting the hull out of the waterline, increasing load on the legs. The first step considered in the operation of a JU is touchdown of the leg on the seabed and afterwards jacking the hull to preloading airgap where load on legs is roughly equal to elevated weight of the JU divided by the amount of legs; 4. The hull is then jacked to preload airgap to minimize wave loading during preloading which introduces additional unwanted vertical leg loads. After jacking to airgap, the preloading procedure is started which ensures enough bearing capacity in the soil is present for later lifting operations due to lifting causing a shift in vertical load on the legs and thus loads to increase past elevated weight divided by 4. But with this preloading, the structure is loaded close to limiting structural conditions of the jacking system which is where the leg and hull are connected to each other and along with leg guides allow for load (vertical and horizontal) and moment transfer which is in turn re-distributed through out the rest of the JU and to other leg-hull interfaces. As safety is a priority in any offshore operation it is essential to comprehend load development and its effect on the structural integrity of JU's.
Clearly defining re-distribution behaviour of loads and moments in a JU and what extra interaction effect a sloped seabed will bring are the main goals of this thesis. This is achieved by creating a geotechnical model describing soil-structure interaction and combining the results with a structural model to create a framework for a JU on a sloped seabed.

1.2. Research questions

Having identified the literature gap in research on JU's on sloped seabeds and determined the scope of this research the main research question can be formulated as follows:

"How does the presence of a sloped seabed influence a four legged jack-up during preloading operation? "

This main research question can then be sub-divided into sub-questions which are aimed at answering a specific section of the main question.

1. How will the presence of a sloped seabed affect the footing response during preloading?
2. How can a structural model be implemented to describe a JU during preloading?
3. How can a framework combining geotechnical and structural domains be employed to obtain loads in a jacking system of a JU during preloading?
4. How does the sensitivity of the model vary with changes in input parameters?

1.3. Methodology

This research comprises of 5 of steps; (1) conducting a literature study to determine what the state-of-art is, (2) developing a soil-structure interaction model for a spudcan on a sloped seabed, (3) developing a structural model to determine global reactions of a JU during preloading which is followed by (4) a combined framework for geotechnical and structural modelling, and finally (5) a sensitivity phase where model parameters can adjusted to analyse separate cases. These steps are crucial in answering the main research question and each of these steps will be highlighted below

1.3.1. Literature review

The main goal here is to report on relevant literature in order to give a strong foundation for the technical background. Firstly, within this technical background an introduction to jack-up vessels with context to its operations is given. The various components that make up a jack-up vessel are introduced and the most essential to the operations are highlighted.
Secondly, the theory behind soil-structure interaction between jack-up and seabed is introduced in order to describe a spudcan on a sloped seabed. The current state-of-art is analyzed to explore previously implemented modelling methods along with their respective advantages and drawbacks.
Lastly, the theory behind modelling a jack-up structure is described in order to adequately model the global behaviour of a jack-up which is preloading on a sloped seabed. The state-of-art is analyzed for combined geotechnical and structural models.

1.3.2. Modelling of soil-spudcan interaction

The geotechnical phase describes the complete aspect of soil-structure interaction of a spudcan on a sloped seabed. To achieve this goal modelling methods are compared and a suitable method is selected and expanded upon. For any model selected, the soil and structure dimensions and parameters must be described along with boundary conditions of the model. Once all these items are defined, load can be applied to the model in order to simulate soil-structure interaction representing a spudcan penetrating a sloped seabed.

1.3.3. Modelling of the JU

The structural phase is oriented around describing the global behaviour of a JU during preloading operations. This is achieved by defining an equivalent JU model which is able to capture all relevant behaviour of a JU while reducing complexity. A suitable modelling method is selected and model parameters such as beam properties and boundary conditions defined. Afterwards calculations can be done and results displayed in the form of displacement and moment plots.

1.3.4. Unification of the two models

This phase encompasses the integration of the geotechnical and structural model into a framework for describing a 4 legged JU on a sloped seabed during preloading. This is achieved by simulating a sloped seabed underneath a leg and cutting that leg out of the structural model at the leg-hull interface and simulating it using a soil-structure interaction model including hull stiffness. A preloading procedure is simulated in the soil-structure interaction model and the reaction loads are re-applied on the now 3 legged JU at the interface. Additionally foundation stiffness' are applied on the remaining 3 legs at the connection to the seabed. With the sloped seabed reaction loads and foundation stiffness', the internal loads occurring during preloading operation give an indication of the effect of the seabed slope on the load distribution within the JU.

1.3.5. Sensitivity analysis

The goal of this phase is to determine the sensitivity of the created framework by varying the input parameters and measuring the difference in response compared to other input values. The sensitivity study is a scientific approach to determine the behaviour of any proposed framework and is done so in this method by varying soil parameters based on relative density and implementing a variation on geometry for soil-structure interaction.

1.4. Thesis outline

- **Chapter 1 - Introduction**
  Provides the reasoning and plan for this research based on defining the problem at hand and a methodology for solving said problem. The problem definition gives a sense of the industry as it currently stands and what operational cases where a knowledge gap exists. The aim then of this research is to bridge the gap by setting up research questions to answer by implementing a methodology.

- **Chapter 2 - Technical background**
  Provides a foundational understanding of JU's, offering insights into their general design, operational principles, modelling methods, and state-of-art. A thorough comprehension of the fundamental workings of a jack-up is essential to contextualize subsequent discussions regarding their interaction with the seabed and preload capacities. The modelling methods are divided into two main domains: geotechnical and structural, as per domain various methods are then described along with the current state-of-art.

- **Chapter 3 - Modelling**
  Firstly the chapter discusses the framework which is set-up in order to answer the research question and to clearly define modelling goals for geotechnical and structural models.
  Secondly, this chapter delves into the domain of geotechnical modelling, focusing on describing the selected modelling method along with a solid argumentation for the selection of parameters. The essence of this chapter is to incorporate a sloped seabed into a geotechnical model and retrieve relevant results describing the load-displacement behaviour for a footing on a sloped seabed.
  Finally, this chapter describes the domain of structural modelling, with the aim of describing global behaviour of a JU during operation.

- **Chapter 4 - Results**
  Shows the results obtained from implementing the framework by first assessing the geotechnical aspects followed by structural results. Each of the aspects of the framework is also validated or compared to industry standards to ensure validity of results.

- **Chapter 5 - Conclusion**
  Takes the research questions along with the results and draws conclusions to the questions based on the results obtained.

- **Chapter 6 - Discussion & Recommendations**
  Takes the conclusions and discusses their implications in the broader sense of the research domain for JU behaviour. Additionally this chapter includes discussion of assumptions made in the set-up of the models for geotechnical and structural domains and gives recommendations for further research.

2

Technical background

This chapter will aim at describing the technical background needed in order to execute research according to the methodology. This is done by first describing the general workings of a JU, followed by geotechnical and structural theories which are implemented to describe a JU on a sloped seabed.

2.1. General information on JU's

This section focuses on defining a JU and it's function by looking back at the history of the elevating platform, describing main components and operations that the JU performs.

2.1.1. History of JU's

In the present day there are many different types of jack up vessels which serve many different functions. These functions include drilling for natural resources, installation of offshore wind turbines and delivering equipment for maintenance. The first three legged JU was the Scorpion which was used to drill for oil in the Gulf of Mexico.

Figure 2.1: First JU, Scorpion built for Zapata Offshore, built in 1955 [16]

As the oil and gas sector grew so did the JU's with the largest JU having legs of 214 metres tall. But recently with the renewable sector growing so did the demand for a stable platform to install wind turbines. This is where the wind turbine installation vessels (WTIV) comes into play, with the first of these vessels being the MPI Resolution Figure 2.2. A vessel with 6 legs and a hydraulic jacking system. The next generation is scaling up to meet the growing demand of larger offshore wind turbines.

Figure 2.2: MPI Resolution installing wind turbines [18]

2.1.2. Main components of a JU

As some terms were mentioned before in the history of JU's it is important to know what the main components of a JU are to understand how such a vessel operates. The main components of the vessel are hull, legs, jacking system, and spudcans.

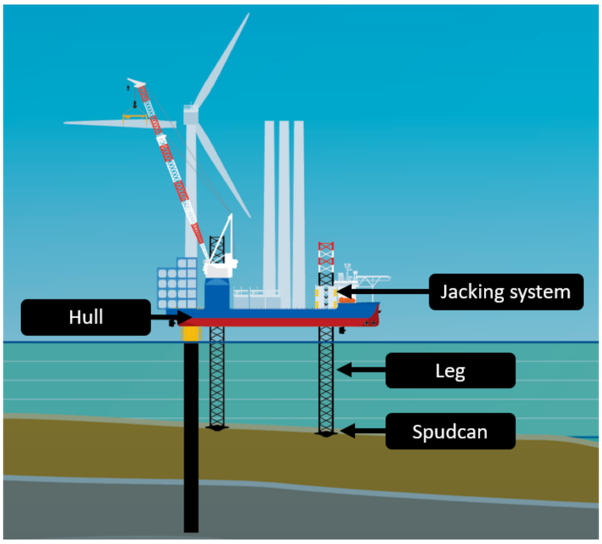

Figure 2.3: Overview of main components of a JU

Hull

The main component of any vessel is its hull which allows a vessel to stay afloat. Traditionally JU rigs are often not self-propelled and must be towed out to location which is not much of a problem as the operation of drilling wells could take up to a year. But with the application of JU's in the offshore wind market, the vessels have a quick turn-around time and must be able to quickly go from one location to another to increase productivity. This caused for the JU's to adopt a more slender ship shaped hull. This can clearly be seen when comparing drilling rigs 2.4 and modern WTIV's 2.2.

Legs and jacking system

There are 2 main leg types when it comes to JU's; cylindrical and truss legs. Where the cylindrical legs are constructed by rolling large steel plates and welding them together to form a large hollow cylinder. In the cylinder there are holes present in which the hydraulic jacking system engages to lift the hull above the waterline. The truss legs comprise of 3 chords with steel braces in between. These braces come in different types: X-braces and K-braces. On the chords themselves a tooth rack is present which is connected to the jacking system. The jacking system consists of pinions on either side of a chord and are powered by electric motors through a transmission.

Spudcan

To keep the legs from penetrating too far into the soil spudcans are added to the ends of the legs of jack ups. These spudcans are very stiff steel structures which penetrate into soils and transfer loads between the soil and structure.

(a) (b)

Figure 2.4: JU vessel (a) and spudcan (b)

The spudcans have a conical shape to allow for a degree of vertical penetration into the seabed which will increase fixity with the soil until the spudcan is fully embedded into the soil. This fixity will in turn ensure a strong connection between the soil and structure and ensure a stable working platform.

2.1.3. Operations

The installation and operation of a JU on location can be characterized by 5 different steps as can be seen in Figure 2.5. And can be summarized in the following steps:

I. Arriving to location

II. Touchdown

III. Jacking to preloading airgap

IV. Passive preloading

V. Jacking to operational airgap

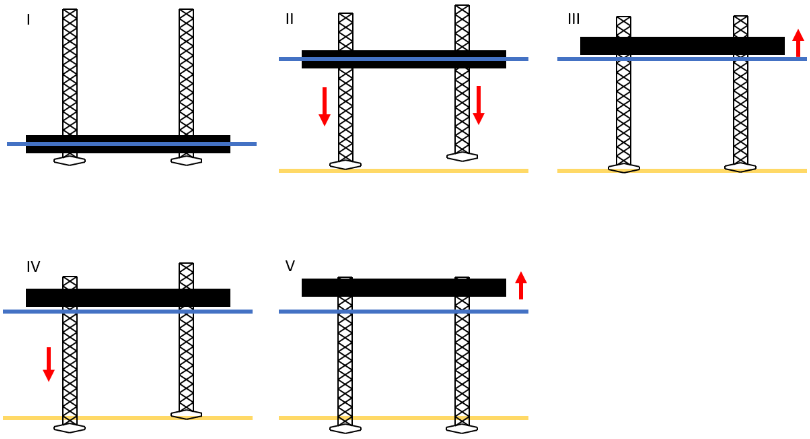

Figure 2.5: Operations for installation of a JU

When a vessel arrives on location the legs are lowered to make contact with the seabed. This initial contact is called touchdown of the spudcan. Once all four legs make contact with the seabed, the legs are pushed down by the pinions in order to jack the hull above the waterline to preload airgap, typically 1-1.5m above the waterline, such that if rapid settlement were to occur, the hull picks up buoyancy rather quickly. Once the required airgap is reached, the preloading process is initialized where opposite diagonal legs form a leg pair (LP); leg pair 1 (LP1) and 2 (LP2). The definition of LP is displayed in Figure 2.6, with LP1 (purple) and LP2 (yellow) being opposite diagonal leg pairs. For passive preloading, the loading LP is put on brakes while the unloading LP is pulled back up. This will cause the vertical reaction to decrease in the unloading LP and an increase for the loading LP. The increase in load will cause the spudcan to further penetrate the seabed. Once a certain preload is reached the roles of the LP's will switch to achieve a preload level in the previously passive pair. This switching is repeated until both LP's have reached a required preload and there is no further settlement of the legs. The preloading process is graphically given in Figure 2.6, where a modified graph from Sonnema 2023 is implemented describing LP1 and LP2 during preloading. The vertical displacement and load on the legs are monitored on the vessel to ensure a safe installation of the JU. If the measured values are coherent with the predicted soil calculations made then the operation may continue and the vessel is jacked to airgap and lifting operations can be started.

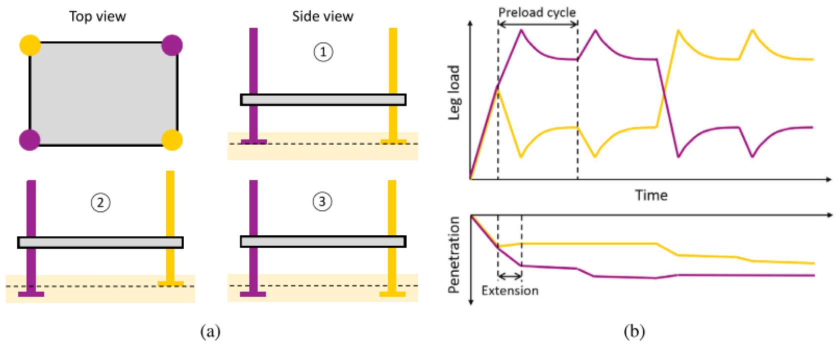

Figure 2.6: Preloading operation with LP's (a) and load and penetration behaviour over time (b) modified Sonnema (2023) [28]

The role of preloading for a JU is to ensure enough soil capacity for certain leg loads to occur during operation and storm conditions [21]. This operation can be seen as a step-wise operation where the load is built up to decrease risk of damage, so per step of preloading, the targeted preload is built up to the maximum target preload. For example the heavy lift JU NG-20000X has a maximum preload of 20,000 tonnes per leg, instead of letting the loaded pair go up to the the maximum, a percentage of target preload will be achieved initially.

2.1.4. Environmental loads

During operations the JU is positioned in at location and is designed to withstand environmental conditions, and depending on the types of conditions operations can be executed when the weather window allows. Here 2 types of weather conditions are defined, operational and storm conditions. The environmental loads that occur on any offshore structure are due to wind, wave and current loading. The calculations for wind and wave loads are kept out of the scope of this research but representative load levels are given as a load on the lower guide ($200 - 600\ MNm$) for operational and storm conditions.

2.2. Soil-structure interaction

In order to understand soil behaviour to model the loading of a spudcan on a sloped seabed, some background information is needed. This chapter will dive into the soil classification, behaviour, constitutive models, foundation capacities and soil-structure interaction models, in order to lay the foundation for geotechnical knowledge applied in this report.

2.2.1. Soil classification

The two main soil types that are covered in the project are sand and clay soils. Sand soils are classified as relatively large particles ($0.2\,mm \leq x_{particle} \leq 2\,mm$) which have a high permeability while clay soils have relatively small particles ($x_{particle} \leq 0.002\,mm$) and a low permeability.

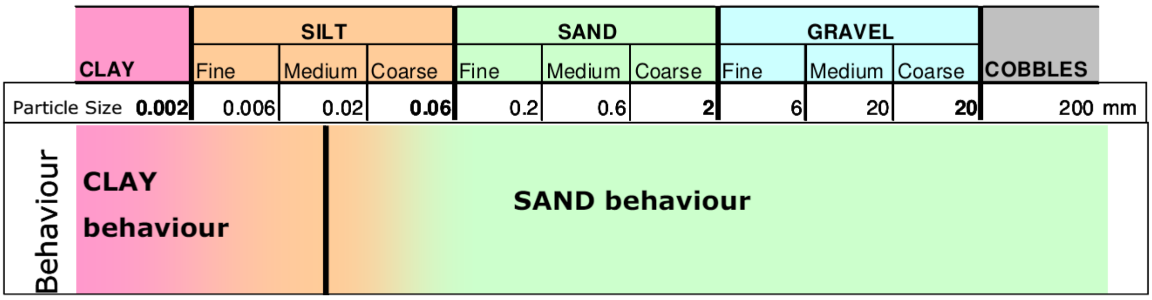

Figure 2.7: Soil classification and behaviour based on British Standard 5930 [31]

Permeability of the soil describes the ability of a soil to allow fluids to flow through itself with sand having a high and clay a low permeability. The high permeability of sand allows for the assumption of drained behaviour under loading. As the high permeability allows for water to easily pass through the sand, the assumption is made that upon loading of a sandy soil, the water is instantaneously drained from the soil skeleton.
As for clayey soils the low permeability causes the water to slowly permeate through the soil skeleton over time upon loading, adding time-dependent reaction.

2.2.2. Basic soil mechanics

Soil behaviour refers to the response of a soil medium upon loading and can be referred to as the amount of strain of a soil medium under a certain stress. This section will delve into the definition of stress and strain in soil and certain parameters used to describe this behaviour.

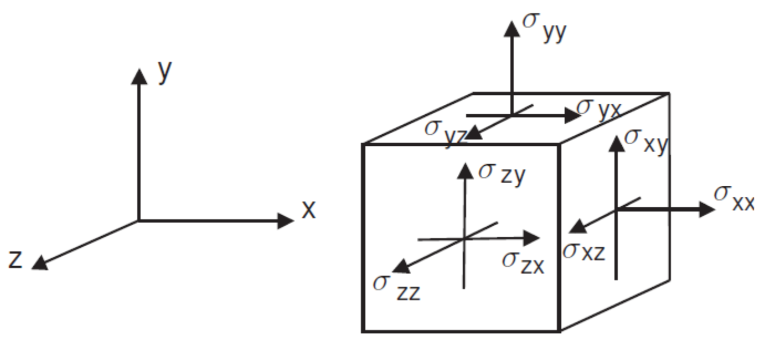

Figure 2.8: General three-dimensional coordinate system and sign convention for stresses [6]

General definition of stress

For a selected soil medium under load, a section can be selected and stress in 3 directions can be seen, the stress can therefore be described by a 3rd order tensor. In this tensor the diagonal terms are equal to the purely compressive stresses and off-diagonal terms equal shear stresses.

$$\sigma = \begin{bmatrix} \sigma_{xx} & \sigma_{xy} & \sigma_{xz} \\ \sigma_{yx} & \sigma_{yy} & \sigma_{yz} \\ \sigma_{zx} & \sigma_{zy} & \sigma_{zz} \end{bmatrix} \tag{2.1}$$

As can be seen in the tensor above, the stress tensor is described in Cartesian coordinates, but often principle stresses are modelled over Cartesian stresses. Principle stresses are aligned in such a way that all shear stress components are zero. Principle stresses are actually the eigenvalues of the stress tensor and can be determined using the formulation for an eigenvector.

$$det(\sigma - \sigma I) = 0 \tag{2.2}$$

For a 3rd order stress tensor this results in 3 eigenvalues which are sorted algebraically with σ_1 being the largest principal stress and σ_3 being the smallest.
In addition to principal stresses, invariants of stress can also be defined in order to describe the stress of a system independent of the orientation of the coordinate system. Two invariants are isotropic effective stress (p') and equivalent shear stress (q).

$$p' = \frac{1}{3}(\sigma'_{xx} + \sigma'_{yy} + \sigma'_{zz}) \tag{2.3}$$

$$q = \sqrt{\frac{1}{2}((\sigma'_{xx} - \sigma'_{yy})^2) + (\sigma'_{yy} - \sigma'_{zz})^2) + (\sigma'_{zz} - \sigma'_{xx})^2) + 6(\sigma^2_{xy} - \sigma^2_{yz} + \sigma^2_{zx}))} \tag{2.4}$$

An important quality of equivalent shear stress (q) is that when $\sigma_2 = \sigma_3$ the equation reduces to a simpler form.

$$q = |\sigma'_1 - \sigma'_3| \tag{2.5}$$

General definition of strain

Strain can be seen as a 3rd order tensor with a Cartesian coordinate system with same sign convention as 2.8. Where strains are defined as the derivatives of the displacement components.

$$\epsilon = \begin{bmatrix} \epsilon_{xx} & \epsilon_{xy} & \epsilon_{xz} \\ \epsilon_{yx} & \epsilon_{yy} & \epsilon_{yz} \\ \epsilon_{zx} & \epsilon_{zy} & \epsilon_{zz} \end{bmatrix} \tag{2.6}$$

$$\epsilon = \frac{1}{2}(\frac{\partial u_i}{\partial j} + \frac{\partial u_j}{\partial i}) \tag{2.7}$$

In this formula i and j refer to the Cartesian coordinates x, y and z. In order to describe the strain of a soil independent of orientation of the coordinate system, invariants are used; volumetric strain (ϵ_V) and deviatoric strain (ϵ_q). Where volumetric strain is equal to the sum of all normal strain components when considering small strain deformation theory.

$$\epsilon_V = \epsilon_{xx} + \epsilon_{yy} + \epsilon_{zz} = \epsilon_1 + \epsilon_2 + \epsilon_3 \tag{2.8}$$

As can be seen the volumetric strain is equal to the sum of all principal strains, which are the eigenvalues of the strain tensor.

$$\epsilon_q = \sqrt{\frac{2}{9}((\epsilon_{xx} - \epsilon_{yy})^2 + (\epsilon_{yy} - \epsilon_{zz})^2 + (\epsilon_{zz} - \epsilon_{xx})^2) + \frac{1}{3}(\gamma^2_{xy} + \gamma^2_{yz} + \gamma^2_{zx})} \tag{2.9}$$

Again as with stress, if $\epsilon_2 = \epsilon_3$, the deviatoric strain will simplfy.

$$\epsilon_q = \frac{2}{3}|\epsilon_1 - \epsilon_3| \tag{2.10}$$

Compressive behaviour

Soil response can be characterized by means of classical theories which state that soil response can be sub-divided into compressive and shear behaviour. [25], [26]. When a soil is loaded causing an increased compressive stress, the soil response can be divided into 3 parts:

- Initial elastic compression
- Primary compression (consolidation)
- Secondary compression (creep)

The response differs per soil type, for sandy soils, where permeability is high, all compression will take place immediately. But in clay soils where permeability is low, the response is divided into two sections, elastic compression and time-dependent compression (consolidation and creep). Consolidation is time dependent due to the dissipation of non-equilibrium pore water pressure causing soil to deform. So when soil with a low permeability is loaded, this is said to be undrained due to the water still being present and a small initial volume change will occur. Only over time the liquid will be forced out of the pores until eventually the load is carried out by the soil skeleton. The volume decreases as liquid is expelled causing extra settlement. On the other hand there are drained conditions where the load is instantaneously carried by the soil skeleton, this can be the effect of high permeability or high load. Creep in soils can be characterised as the deformation which occurs under constant effective stress for an extended period of time.
In order to determine the compressive behaviour of soils, soil testing can be applied in the form of consolidation tests. These consolidation tests are implemented using an oedometer test, in which a vertical load is applied to a soil medium often in steps to determine the stress-strain behaviour of that soil. The one dimensional oedometer elastic modulus is determined by the change in vertical effective stress over change in vertical strain [23].

$$E_{oed} = \frac{\Delta\sigma_1}{\Delta\epsilon_1} \tag{2.11}$$

Compressive behavior gives way to elastic theory which is applied to describe soils. The elastic response of an isotropic material is described by Young's modulus (E) and Poisson's ratio (v). The Young's modulus is given by the ratio of change in deviatoric stress and vertical strain.

$$E = \frac{\Delta q}{\Delta\epsilon_1} \tag{2.12}$$

Poisson's ratio can be defined by the ratio of an increment of lateral strain to vertical strain.

$$v = \frac{-\Delta\epsilon_3}{\Delta\epsilon_1} \tag{2.13}$$

Now a relation between the oedometer stiffness and Young's modulus can be made as follows.

$$E_{oed} = \frac{\Delta\sigma_1}{\Delta\epsilon_1} = \frac{(1-\nu)E}{(1-2\nu)(1+\nu)} \tag{2.14}$$

Shear behaviour

Another soil response to loading is shear, which a soil can resist through friction. The shear strength (τ_f) on a potential failure plane is a function of normal effective stress (σ') on that failure plane and effective internal friction (ϕ). These parameters can be formulated as the effective stress failure criterion.

$$\tau_\mathrm{f} = \sigma' \tan\phi \tag{2.15}$$

This stress failure criterion - also known as Mohr-Coulomb (MC) failure criterion - can be implemented to determine when a combination of loads causes failure to occur in a soil medium, which is useful when implementing soil constitutive models, as done in subsection 2.2.3. The MC failure criterion refers to the combination of a Mohr circle and Coulomb friction to determine when soil failure occurs. The Mohr circle describes a combination of normal and shear stress of a soil sample.

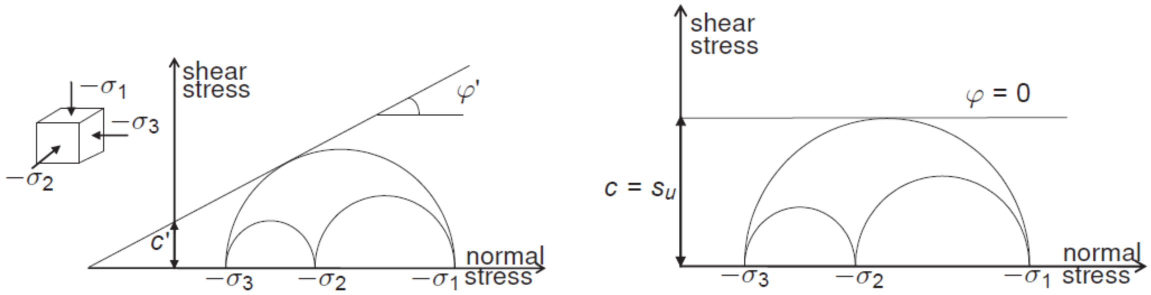

Figure 2.9: Mohr circles for drained (left) and undrained (right) soils

The Mohr-circles above show the stress states of a soil sample, defined by maximum (σ_1) and minimum (σ_3) principal stresses, and a failure line given by Coulomb friction, defined by internal friction angle (ϕ) of soil and cohesion (c). Here the failure function (f) is a mathematical formulation for a combination of stress states and strength parameters and when the failure function equals 0, failure occurs.

$$f = \frac{\sigma_1' - \sigma_3'}{2} + \frac{\sigma_1' + \sigma_3'}{2} sin(\phi) - ccos(\phi) \leq 0 \tag{2.16}$$

Shearing of a soil causes a volumetric change to occur in soil with either contraction or dilation occurring, which refer to the decrease and increase in volume respectively. This change in volume occurs as a soil volume can be viewed as an arrangement of particles and in order for one part of the arrangement to move over another, the particles must be re-aranged. The volume at which constant shear of one part of the arrangement over another can occur takes place at a certain critical void ratio (e_{cr}). If the arrangement of particles is more loosely packed than the critical void ratio, then contraction will occur before constant shearing and if more densely packed than the critical void ratio, then dilation will occur.

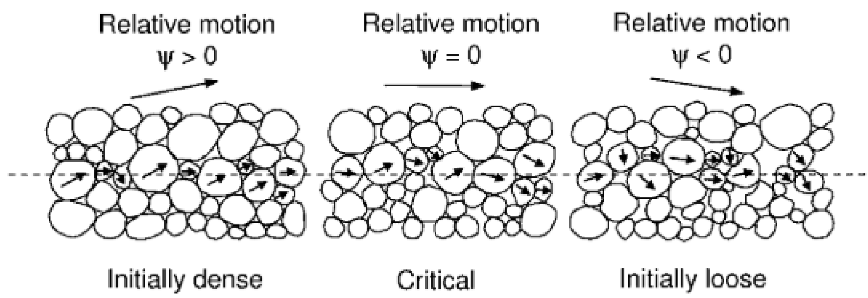

Figure 2.10: Dilation and contraction during shearing [4]

The dilation angle is equal to the angle between the planes between particle that need to move over one another. This can be explained with the analogy of a saw tooth model where the effect of dilation angle is highlighted.

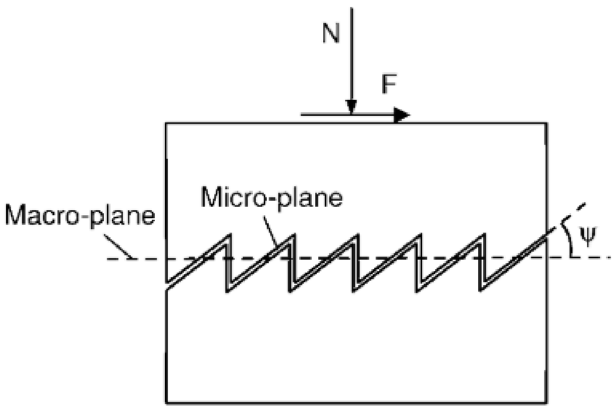

Figure 2.11: Saw tooth model of dilation [4]

Here the macro-plane is aligned with the critical internal friction angle of the soil medium, the top layer is loaded with vertical force N and has shearing resistance F. An additional resistance is needed as the top layer of teeth need to ride over the bottom layer, where the angle is equal to the dilation angle (ψ). This angle determines the additional amount of additional load needed to mobilize the soil, which brings the apparent friction angle to a higher value of peak friction angle (ϕ_p).

$$\phi_p = \phi_{cr} + \psi \tag{2.17}$$

2.2.3. Soil constitutive models

Soil can deform in 2 primary ways, elastic and plastic deformations. In reality these 2 deformations will occur simultaneously causing an elastic-plastic response. When a soil is initially loaded the soil will deform elastically until a threshold is reached, which is called the yield point. If unloading were to occur before the yield point is reached the soil would fully recover to its initial state. However when the load exceeds the yield point, the soil will enter plastic deformation (ϵ_p). When the soil is unloaded, the soil will not return to its initial state and a permanent deformation will occur. This behaviour can be seen in Figure 2.12 where the unloading point will not be the same as the initial state.

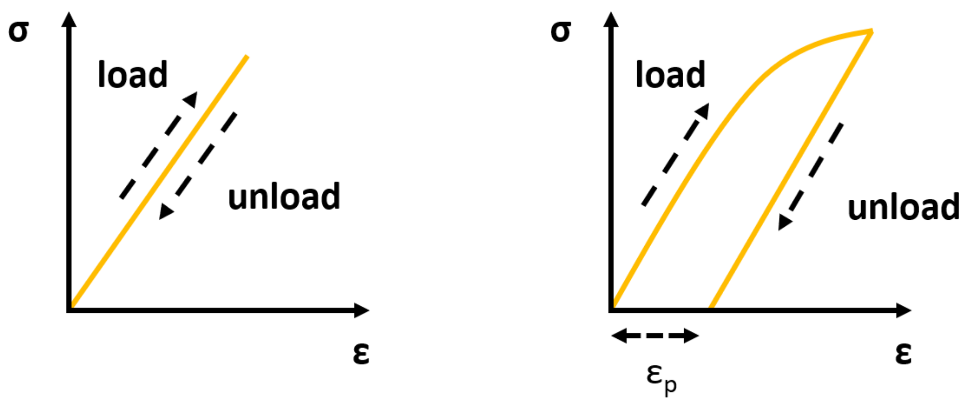

Figure 2.12: Stress-strain curves for linear (left) and non-linear (right) scenarios

The elastic and elastic-plastic theories give a relation between stress and strain with elastic-plastic theory including failure, this mathematical relation can also be referred to as the constitutive model. Constitutive models vary depending on what effects are included, for a Linear Elastic (LE) constitutive model, a linear relation between stress and strain is assumed with infinite strength. The second constitutive model taken into consideration is an elastic-perfectly plastic model; Mohr-Coulomb (MC) constitutive model takes soil failure into account using the MC failure criterion. The third type of constitutive model taken into consideration has the ability to model hardening of soil as is referred to as the Hardening Soil (HS) constitutive model.

Linear Elastic (LE)

The LE soil constitutive model is based on Hooke's law of isotropic linear elastic behaviour and is applied as an initial estimation for soil stress strain behaviour, as it is not possible to model non-linearities due to soil failure or hardening. The conventional formulation for Hooke's law in geotechnical problems is done so using derivatives of stress and strain and is expressed as follows:

$$\dot{\sigma} = \mathbf{D}^e \dot{\epsilon} \tag{2.18}$$

$$\begin{bmatrix} \dot{\sigma}'_{xx} \\ \dot{\sigma}'_{yy} \\ \dot{\sigma}'_{zz} \\ \dot{\sigma}'_{xy} \\ \dot{\sigma}'_{yz} \\ \dot{\sigma}'_{xz} \end{bmatrix} = \frac{E}{(1-2\nu)(1+\nu)} \begin{bmatrix} 1-\nu & \nu & \nu & 0 & 0 & 0 \\ \nu & 1-\nu & \nu & 0 & 0 & 0 \\ \nu & \nu & 1-\nu & 0 & 0 & 0 \\ 0 & 0 & 0 & \frac{1}{2}-\nu & 0 & 0 \\ 0 & 0 & 0 & 0 & \frac{1}{2}-\nu & 0 \\ 0 & 0 & 0 & 0 & 0 & \frac{1}{2}-\nu \end{bmatrix} \begin{bmatrix} \dot{\epsilon}_{xx} \\ \dot{\epsilon}_{yy} \\ \dot{\epsilon}_{zz} \\ \dot{\gamma}_{xy} \\ \dot{\gamma}_{yz} \\ \dot{\gamma}_{xz} \end{bmatrix} \tag{2.19}$$

Two main parameters for describing the LE model are Young's modulus of elasticity (E) and Poisson's ratio (ν), as can be seen in $\mathbf{D}^e$ above. A set of alternative elastic parameters can be defined in order to isolate volumetric and shear behaviour of the model.
Shear modulus is a value that combines Young's modulus and Poisson's ratio to describe change in shape of soil due to shear at a constant volume.

$$G = \frac{E}{2(1+\nu)} \tag{2.20}$$

The second alternative parameter is the bulk modulus which describes the volumetric strain due to change in isotropic effective stress.

$$K = \frac{E}{3(1-2\nu)} \tag{2.21}$$

These physical interpretation behind these values can be seen in Fig 2.13 where Young's modulus describes the change in length in (b) and Poisson's ratio the change in width. The shear modulus describes the change in shape in (c) at constant volume and bulk modulus the change in volume due to change in isotropic effective stress (d).

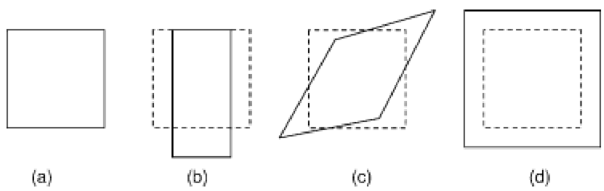

Figure 2.13: Elastic deformations

Using these alternative stiffness parameters that are independent of Cartesian coordinate system by using invariants for stress and strain. Additionally the alternative formulation separately describes compression and shear loading effects as the off-diagonal terms of the stiffness matrix are zero.

$$\begin{bmatrix} \dot{p} \\ \dot{q} \end{bmatrix} = \begin{bmatrix} K & 0 \\ 0 & 3G \end{bmatrix} \begin{bmatrix} \dot{\epsilon}_V \\ \dot{\epsilon}_q \end{bmatrix} \tag{2.22}$$

Mohr-Coulomb (MC)

Soils behave non-linear when subjected to change in stiffness or strain. In reality the soil stiffness is dependent on at least the stress level, stress path and strain level which are included in more advanced soil models. The MC model however is a simple elastic perfectly plastic model which is used for a first approximation of soil behaviour. The elastic part is based on Hooke's law of isotropic elasticity and the perfect plastic part on MC failure criterion.

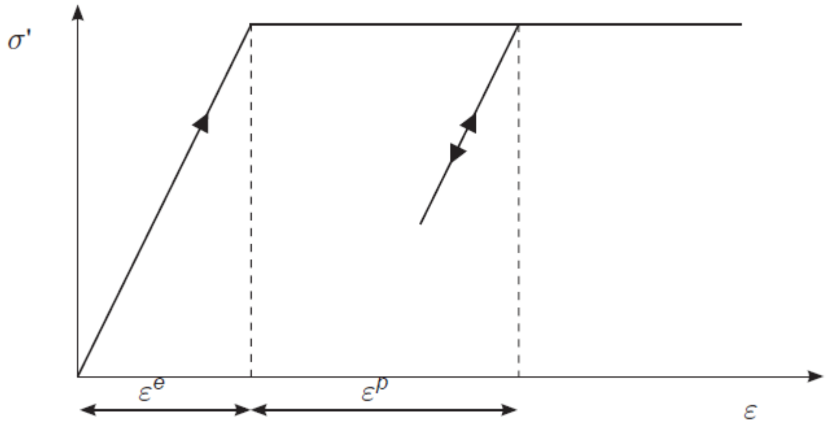

Figure 2.14: Elastic perfectly plastic (MC) soil constitutive model [6]

The combined elastic plastic behaviour is showcased in Figure 2.14 where the stress-strain plot showcases initial linear behaviour (ϵ^e). After a linear increase up to a certain failure point, perfect plastic behaviour will follow where stress cannot be increased but only displacement can occur (ϵ^p). After a given displacement if the stress is reduced, the soil will revert back to linear behaviour upon unloading and reloading.

Plasticity involves the development of irreversible strains and in order to determine plastic strain, a yield function (f) is introduced as a function of stress and strain. Yielding occurs when ($f = 0$) and for a perfectly plastic model, the yield surface remains fixed and is not influenced by further straining.
Hooke's Law can be decomposed into an elastic and plastic part:

$$\dot{\sigma'} = \mathbf{D^e}(\dot{\epsilon^e} - \dot{\epsilon^p}) \tag{2.23}$$

The plastic strain rates (ϵ^p) are proportional to the derivative of the yield function with respect to the stresses, which means the plastic strain rates are represented as vectors perpendicular to the yield surface. This form of theory is referred to as associated plasticity. However another function must be implemented as MC type yield functions (f) overestimate dilatancy, this function is the plastic potential function (g).

$$g = \frac{\sigma_1' - \sigma_3'}{2} + \frac{\sigma_1' + \sigma_3'}{2} sin(\psi) \leq 0 \tag{2.24}$$

This function is dependent on the dilatancy of soil where it describes positive plastic volumetric strain increments for dense soils. So a dense soil that is packed when loaded on will expand volumetrically due to the packed particles moving around.
Now both yield and plastic functions are defined, the relation between effective stress and strain rates can be determined.

$$\dot{\sigma}' = (\mathbf{D}^e - \frac{\alpha}{d}\mathbf{D}^e \frac{\partial g}{\partial \dot{\sigma}'} \frac{\partial f^T}{\partial \dot{\sigma}'} \mathbf{D}^e)\dot{\epsilon} \tag{2.25}$$

Where:

$$d = \frac{\partial f^T}{\partial \dot{\sigma}'} \mathbf{D}^e \frac{\partial g}{\partial \dot{\sigma}'} \tag{2.26}$$

Here the parameter α is used to switch between elastic and plastic behaviour by switching between 0 and 1 respectively. Concluding, the yield function (f) uses MC failure criterion in order to determine if under a given combination of normal and shear stress, failure will occur. Another parameter is included

Hardening Soil (HS)

The third soil constitutive model taken into consideration includes failure according to MC failure criterion along with the stress dependent stiffness of soil causing an increase in accuracy of soil modelling but at the cost of increased complexity.
The Hardening Soil (HS) model determines elastic strain according to Hooke's law but the elasticity is stress dependent. Also the elastic strain parameters differ from previous LE and MC models in that the elasticity is determined by 3 elastic stiffness moduli. The first is the secant stiffness at 50 % of the maximum deviatoric stress (E_{50}) obtained during drained tri-axial testing, the second is the tangent stiffness modulus obtained from oedometer test (E_{oed}) and finally the Young's modulus for unloading and reloading (E_{ur}), which is also obtained through triaxial testing. One basic idea is that the relationship for standard drained triaxial test is hyperbolic. In this test the relation between deviatoric stress (q) and axial strain (ϵ_1) are measured in triaxial loading.

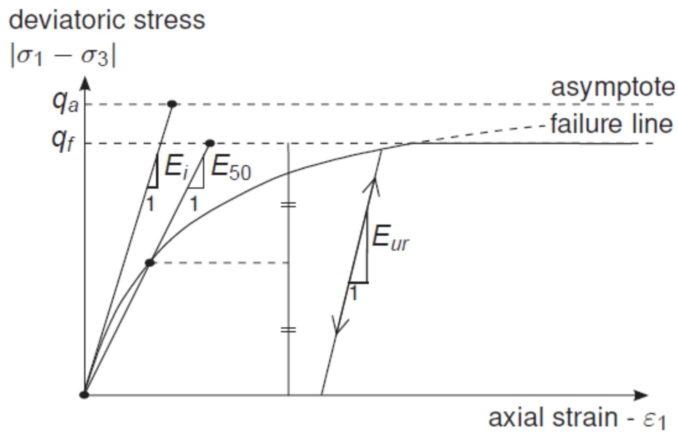

Figure 2.15: Hyperbolic stress-strain relation for standard drained triaxial test [6]

Here the hyperbolic relation can clearly be seen with the test starting in the origin and flowing to the asymptote (q_a), but perfect plastic failure occurs at the ultimate deviatoric stress (q_f) which is determined from the MC failure criterion.

$$q_f = (c\ \cot(\phi - \sigma_3')\frac{2\sin(\phi)}{1-\sin(\phi)} \tag{2.27}$$

Where c, ϕ are soil strength parameters for cohesion and internal friction angle respectively, σ_3' is the minor principal stress. Along with the quantity of the asymptote which is determined by a selected failure ratio (R_f) and ultimate deviatoric stress (q_f).

$$q_a = \frac{q_f}{R_f} \tag{2.28}$$

Implementing the hyperbolic relation the formulas can be determined for E_{50} and E_{ur} by taking an input values of reference stiffness moduli for both values and the following formulas:

$$E_{50} = E_{50}^{ref}(\frac{\sigma_3 + c\,sin(\phi)}{p^{ref} + c\,sin(\phi)})^m \tag{2.29}$$

$$E_{ur} = E_{ur}^{ref}(\frac{\sigma_3 + c\,sin(\phi)}{p^{ref} + c\,sin(\phi)})^m \tag{2.30}$$

The final elastic stiffness modulus is determined from oedoemeter testing for one dimensional compression (E_{oed}).

$$E_{oed} = E_{oed}^{ref}(\frac{\sigma_1 + c\,sin(\phi)}{p^{ref} + c\,sin(\phi)})^m \tag{2.31}$$

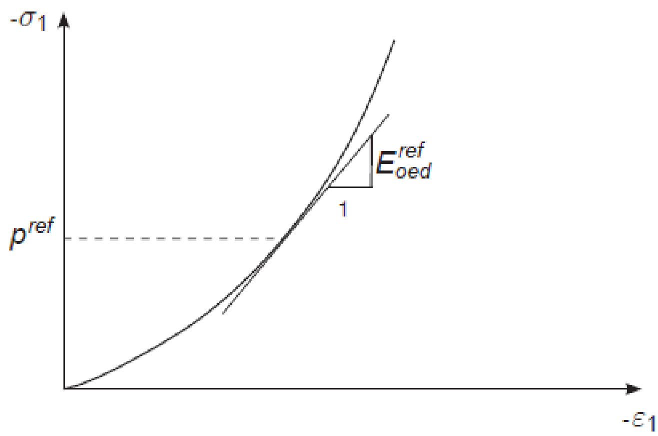

Figure 2.16: Oedometer stiffness defined (E_{oed}) as tangent at reference pressure in oedeometer test [6]

2.2.4. Foundation capacity

Foundation capacity is defined as the maximum amount of load a foundation is able to exert on the surrounding soil before failure occurs, often leading to increased settlement of the footing. This capacity is dependent on the soil type (drained or undrained), embedment depth of load, foundation geometry soil strength parameters.

Vertical bearing capacity

The basis for bearing capacity theory is given by Terzaghi [30] in which the bearing capacity of the soil is determined for a rectangular infinitely long strip footing. Another assumption made is that the footing is shallow and that there is no inclination assumed.

$$q_{ult} = cN_c + \frac{1}{2}BN_\gamma + qN_q \tag{2.32}$$

where:

c	is the soil cohesion (shear strength)
B	is the foundation width
q	is the surcharge
γ	is the soil unit weight
N_c, N_γ, N_q	are the bearing capacity coefficients

Later on Terzaghi's equation was modified by Hansen [12] to include 5 factors to account for shape, depth, load inclination, base inclination and ground inclination. These factors allow for determining bearing capacity for different shapes by introducing effective foundation area which is determined such that the geometric centre coincides with the load centre and the contours are followed as closely as possible.

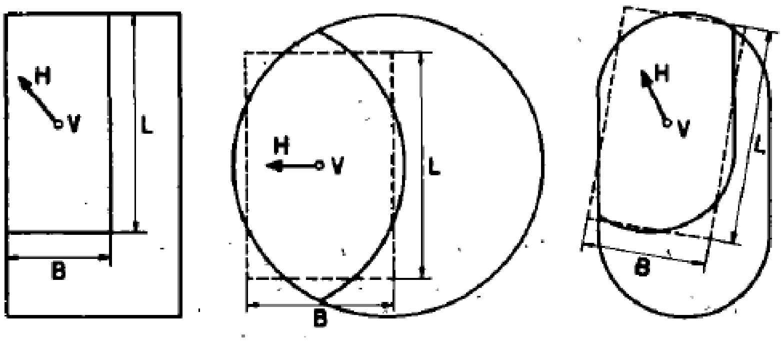

Figure 2.17: Effective area for various foundations

$$q_{ult} = \frac{1}{2}\gamma N_\gamma s_\gamma d_\gamma i_\gamma b_\gamma g_\gamma + qN_q s_q d_q i_q b_q g_q + cN_c s_c d_c i_c b_c g_c \tag{2.33}$$

where:

s	is the shape factor
d	is the depth factor
i	is the load inclination factor
b	is the base inclination factor
g	is the ground inclination factor

The bearing capacity calculation for spudcan in soil follows the classical bearing capacity theory [30], however some modifications have been made. An equivalent undrained shear strength is applied, recommending a shear strength averaged over the zone from spudcan tip to a depth of half a spudcan diameter [23].

$$V = (s_u N_c v + \sigma'_{v0})A \tag{2.34}$$

Solutions for bearing capacity factor N_c are given for spudcan foundations with circular conical shapes of diameter D, cone angles between 60 and 180, different embedment depths (0-2.5 diameters) in soils with different strength gradients [14]. These methods that are used to determine spudcan penetration assume a wish-in-place footing. Caution must be taken when effects such as backflow are introduced due to deep penetration into soft clay soils.

When deep penetration of a spudcan occurs in clay there are extra mechanisms that come into play. The deep penetrations causes soil to flow around the spudcan and to initially heave upwards where with further penetration the cavity left by the spudcan is filled, this phenomena is called backflow. With enough backflow occurring the cavity is filled completely and limits the cavity depth. These steps can be seen in figure 2.18. Cavity depth is estimated by [13]

$$\frac{H}{D} = S^{0.55} - \frac{S}{4} \tag{2.35}$$

$$S = (\frac{s_{um}}{\gamma' D})^{(1-k/\gamma')} \tag{2.36}$$

Where H is the depth of the cavity and D the diameter of the spudcan, γ' is the effective unit weight of soil, k the rate of increase in shear strength with depth and s_{um} a value of shear strength at the soil surface. This can help determine the maximum cavity depth at which point the bearing capacity of soil will be adjusted according to Hossain and Randolph. Soil will start to flow around the spudcan beyond the point of backfill and thus the flow-around can be accounted for in the bearing capacity as

$$V = s_u N_{cd} A + \gamma' V_{spudcan} \tag{2.37}$$

Where $V_{spudcan}$ is the volume of the now embedded spudcan and N_{cd} is estimated by Hossain and Randolph with numerical and experimental values and is represented by

$$N_{cd} = 10(1 + 0.065\frac{w}{D}) <= 11.3 \tag{2.38}$$

with w as spudcan embedment and D spudcan diameter and 11.3 the ultimate fully localised flow-around mechanism.

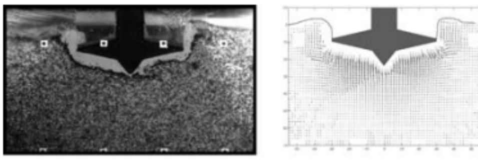

(a) Surface heave mechanism, depth/D = 0.16

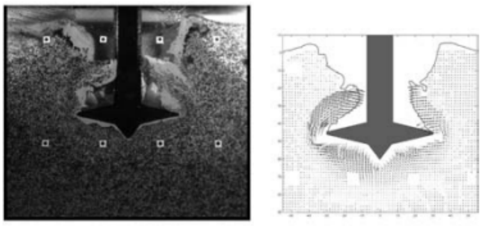

(b) Onset of flow-around mechanism, depth/D = 0.77

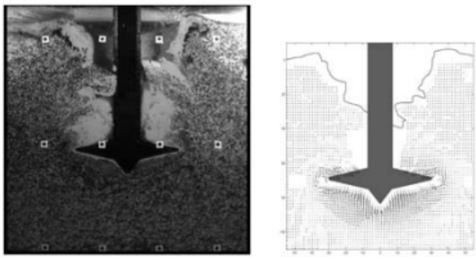

(c) Full flow-around mechanism, depth/D = 1.15

Figure 2.18: Digital images and flow vectors from centrifuge tests (Hossain et al. 2004)

Spudcans penetrating into silica sands are usually viewed as drained conditions as there are no pore water pressures generated.

$$V = \gamma' N_\gamma \pi B^3/8 + p'_o d_q N_q \pi B^2/4 \tag{2.39}$$

Where the first term is always present but the second term is neglected when penetration is minimal and the maximum spudcan diameter fails to come in contact with the soil. This is likely to occur when penetrating into stiff sand soils [23]. In reality the calculation made fails to capture all effects occurring on spudcan and does not take effects such as mobilisation or softening into account, there area a few ways to correct for this behavior. One way is to reduce the internal angle of friction to an estimated mobilisation value. According to industry standards, a reduction of 5 degrees of internal angle of friction is appropriate [9].

Horizontal resistance

Classical bearing capacity theory is useful for determining vertical bearing capacity but does not state anything about horizontal capacity. According to DNV-RP-C-212 (9.2.6.2) the horizontal capacity is equal to the base resistance (R_b) and embedded resistance (R_e) [9]. The former describes the sliding resistance of the base area on the soil, while the latter considers the soil resistance of the side of the embedded spudcan sections.

$$H = R_b + R_e \tag{2.40}$$

For cohesionless sandy soils, the base resistance (R_b) is determined by the formula:

$$R_b = \alpha * tan(\phi)F_v \tag{2.41}$$

The factor α describes the relative roughness between spudcan and soil. For a steel surface industry standards apply a value in the range of 0.6 - 0.8.
The embedded resistance is determined using two different types of pressures, active and passive pressure. The difference in soil pressures is due to the way soil reacts when loaded, with passive referring to the reaction pressure due to an external load from an object and active referring to an active pressure from the soil working on the object. In terms of spudcans: the passive soil pressure is caused by lateral movement of the spudcan in soil where the pressure works in the opposite direction as the movement. The active pressure is caused by the gap created in the soil which is left by the laterally displacing spudcan. The coefficients for passive and active spudcan pressures are dependent on internal angle of friction ϕ.

$$k_p = \frac{1 + sin(\phi)}{1 - sin(\phi)} \tag{2.42}$$

$$k_a = \frac{1}{k_p} \tag{2.43}$$

These coefficients, combined with area, soil weight, and depth contribute to the determination of embedded resistance.

$$R_e = \int_0^z \frac{1}{2}\gamma(k_p - k_a)A(z)dz \tag{2.44}$$

It is essential to note is that the horizontal capacity is a function of both the vertical load and the penetration of the spudcan.

2.2.5. Soil structure interaction modelling methods

Now applying the knowledge obtained about soil response and soil capacity, the question becomes how can this be used to model the response of a soil and structure during loading. There are different methods in modelling soil-spudcan interaction differing in complexity. For this research 3 main methods have been identified.

- Lumped uncoupled foundation stiffness
- Lumped coupled foundation stiffness
- Soil continuum

Lumped uncoupled foundation stiffness

The first method of modelling soil-structure interaction consists of the lumped uncoupled method, which describes the soil as uniaxial stiffness values. This can be achieved by selecting the degrees of freedom (DOF) depending on the type of model used (2D vs. 3D), and creating a stiffness matrix which is diagonally populated, showing uncoupled behaviour.

$$\mathbf{K} = \begin{bmatrix} K_1 & 0 & 0 \\ 0 & K_2 & 0 \\ 0 & 0 & K_3 \end{bmatrix} \tag{2.45}$$

These stiffness values can be determined using industry standards [21], which are a set of empirical formulas describing foundation stiffness during linear operation of a structure on a flat seabed. The linear spring stiffness can be calculated for vertical, horizontal and rotational directions.
For determining the vertical, horizontal and rotational stiffness for elastic solutions with modification factors to account for spudcan embedment, the following formulas can be used.

$$K_1 = K_{\text{d1}} \frac{2GB}{(1 - v)} \tag{2.46}$$

$$K_2 = K_{d2}\frac{16GB(1-v)}{(7-8v)} \tag{2.47}$$

$$K_3 = K_{d3}\frac{GB^3}{3(1-v)} \tag{2.48}$$

Here G is the shear modulus of the foundation soil, v is Poisson's ratio, B is the maximum effective spudcan diameter in contact with soil, K_{d1}, K_{d2} and K_{d3} are stiffness depth factors. These stiffness depth factors take the effect of embedment into account by increasing stiffness as depth increases and is based on a finite element research conducted by Bell (1991) [3]. One important note is that these conditions are for a spudcan that is operating in an elastic soil region, meaning that no plastic effects are taken into account. This implies that when plastic soil deformation is taking place, the stiffness of soil cannot be described by the stiffness presented by ISO.

Lumped coupled foundation stiffness

The second method of modelling soil-structure interaction consists of lumped coupled foundation stiffness, which unlike the previous method, introduces coupled stiffness values. This method is referred to as the macro element (ME) and captures coupling effects of soil-structure interaction that translates to lateral displacement and rotation due to a vertical load for example. To be able to capture non-linear effects as lumped linear springs, the macro element (ME) models are applied, also known as force-resultant models, which describe the foundation response through a relationship between loads (static) and displacement (kinematic) variables. [22].

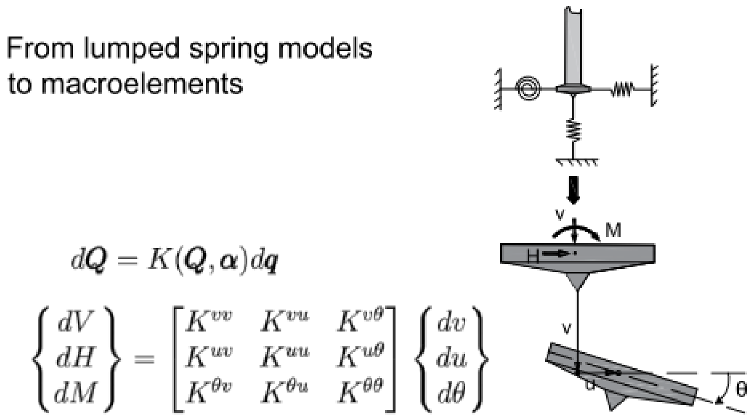

Figure 2.19: Lumped springs to macro element model of a 2D spudcan Pisano (2019)

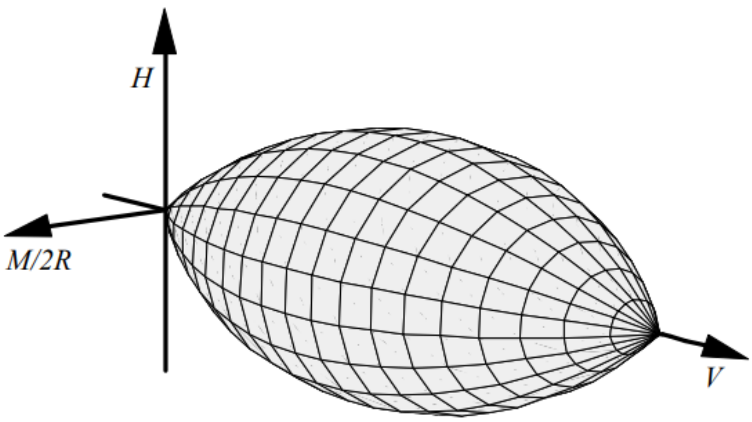

Figure 2.20: Yield surface depicting cigar shape (Cassidy 1999)

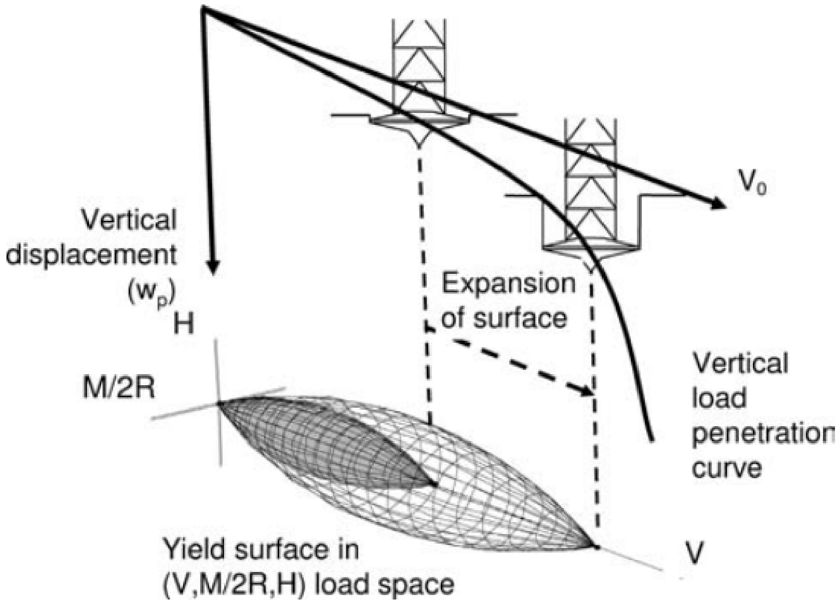

Figure 2.21: Expansion of combined yield surface

One type of these models is a plasticity based force-resultant model in which strain hardening effect of soil is taken into account. These models are often referenced as Model C and contain four main components [7].

- A formulation of the yield surface which gives the boundary for elastic and plastic deformation
- A strain hardening law describing the evolution of the yield surface under plastic deformation
- Description of load-displacement behaviour
- A flow rule to predict footing displacements during yield

Determining the foundation capacity is historically done by empirical methods ([12]) and determine the effect of vertical, horizontal and moment load on the vertical bearing capacity. These methods are replaced by equations where the yield surface is written directly in terms of vertical, horizontal and moment load components. The general shape of this surface is found to be cigar shaped and can be seen in figure 2.20. This shape can be backed up by experimental data obtained for spudcan soil capacities by means of swipe tests [11].
The strain hardening law will describe the change in yield surface due to plastic deformation. This change of yield surface occurs at constant shape and is determined by V_0 which is the maximum vertical load applied such as a preload. This expansion of the yield surface at constant shape can be seen in figure 2.21.
The last two steps involved in Model C are to determine a set-up of a linear elastic force displacement relationship and a relation between plastic displacements.

Continuum model

The most complex method to be discussed is a continuum model of the soil. This is chosen to be able to model non-linearities for strain levels of the soil. These types of models however cost a significant amount of time to set-up and are computationally expensive. Continuum models can be divided into two main groups small strain finite element (SSFE) and large deformation finite element (LDFE) models. The basic workings of finite element models are that a geometry is defined, a mesh is created by dividing the geometry into nodes and elements connecting the nodes, boundary conditions are applied where relevant and calculations are then performed.
For SSFE models, the main assumption is that the strain of the model remain small such that the mesh only needs to be determined once, before any calculation is made. This allows for relative quick calculation time but does not allow for modelling large strains, where nodal displacements can become larger than element sizes. Another type of continuum models are large deformation models which have

the ability to model large displacements. As stated before; traditional FE models are developed based on the assumption of small displacements. This is done as the material can be assumed as linear, which simplifies calculations by removing non-linear terms. Another reason is that these traditional FE models are applied in structural analysis where small displacement are common. But modern FE codes are able to process data such that complex large deformations are able to be modelled using LDFE.
Within LDFE modelling there are models being applied to model spudcan penetration into soil: Coupled Eulerian Lagrangian (CEL) [34], [15], [27] and Arbitrary Lagrangian-Eulerian (ALE) [32] methods. Due to the availability of software containing CEL, only this LDFE method will be discussed. For modelling in CEL, the relatively rigid structure of the spudcan is modelled as a Lagrangian body and the softer soils as Eulerian materials. A contact algorithm is implemented to describe friction between the two material types. In this modelling method soil constitutive models are applied to model plastic behaviour of soil [33].

2.2.6. Soil Spudcan Interaction state-of-art

Historically speaking JU's have been around since the 1950's, and have since then been researched in order to understand working principles and to allow designs of these vessel to become larger and reach new depths. Adding to any research topic needs an analysis of the state-of-art in that research field in order to prevent any overlap in research. The state-of-art which will be analysed focuses on spudcan interaction with the seabed and especially sloped seabeds. The first paper analysed is about the penetration of a spudcan into a sloped seabed. Spudcan penetration as discussed before is a plastic deformation, which means the soil fails, this occurs until the capacity at a certain depth is larger than the loads occurring and a new equilibrium is reached. To analyse this behaviour, a numerical and experimental study were conducted where a spudcan is penetrated into a sloped seabed [27]. This research points out that with an increased seabed slope the lateral resistance of the soil also increases. This is confirmed in both numerical (LDFE) and experimental (centrifuge) results 2.22.

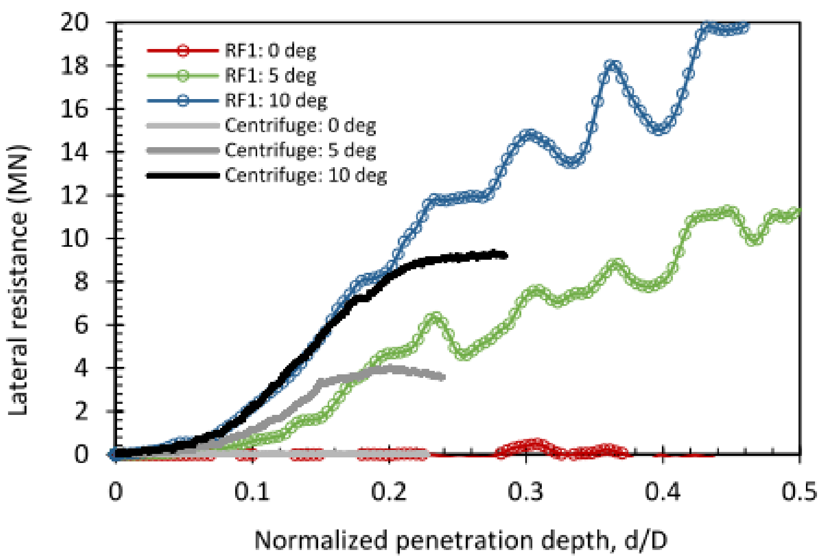

Figure 2.22: Lateral penetration resistance versus normalized depth, Shin (2021)

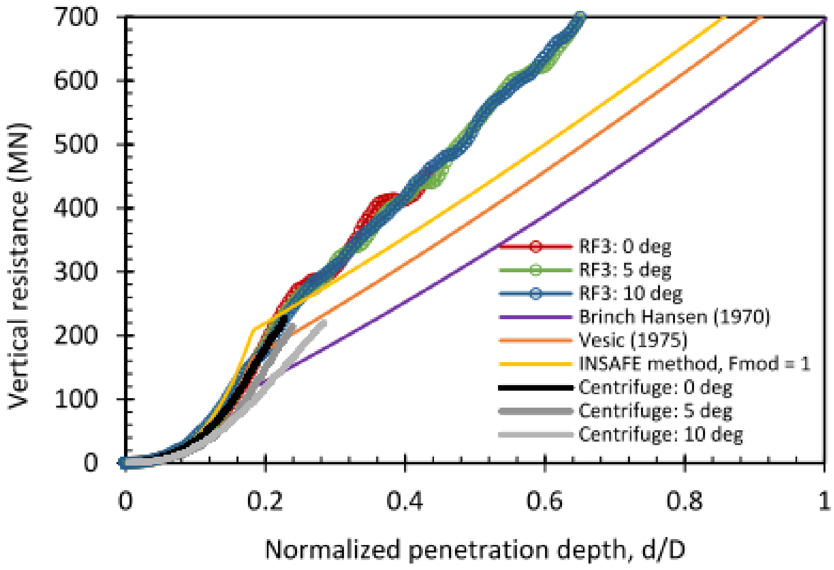

Figure 2.23: Vertical penetration resistance versus normalized depth, Shin (2021)

Another observation from both analyses is an asymmetric failure curve in the soil, this asymmetric failure will lead to an eccentric vertical loading on the spudcan and a horizontal displacement downhill of the slope. The eccentric vertical loading can be compared with the effective area determined in figure Figure 2.17.
One important assumption made in this research is that the lateral displacement is fixed, causing high loads to occur. Another interesting finding in this paper is that a good agreement between classical bearing capacity analysis and large deformation finite element modelling is found until the base of the spudcan comes into contact with the soil.
The second paper taken into consideration is done so by analysing a spudcan on a sloped seabed which is induced by a footprint, which is left by a spudcan which has previously been installed. The initial goal is to always avoid installation of a JU next to a footprint, but this cannot always be done so research is done on the effect of interaction between footprint and spudcan Figure 2.24.

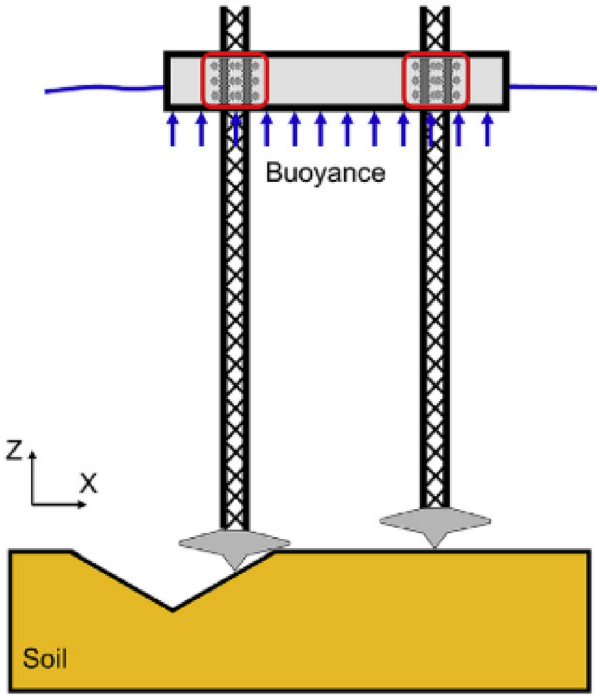

Figure 2.24: Schematic of a JU installation next to a footprint [15]

This research applied different preloading strategies for a 3 legged JU; 'normal' preloading where one leg is penetrated and the others stay stationary, and simultaneous preloading where all legs penetrate simultaneously. Soil-structure interaction is captured by implementing a LDFE (CEL) model. Important interactions were captured such as horizontal sliding of the spudcan into the footprint, overturning of the JU and structural failure.
The use of CEL enables for penetration of the soil to be analysed accurately and a nonlinear stiffness to be determined for vertical and lateral displacement and rotation. This is because the load and displacements are known and plotted in a graph to create an overview of the stiffness of the soil. An important aspect of these results is the increase and decrease of eccentricity of the vertical load. As initial penetration occurs on the sloped seabed, the eccentricity is largest and as further penetration of the spudcan occurs, the vertical load will increase but the eccentricity will decrease. This increase in load and decrease of eccentricity cause the maximum moment occurring in the spudcan to not be when the load is at its largest but when the combination of load and eccentricity are at their largest. So the largest moment occurring during preloading does not necessarily occur at final penetration depth.
One of the main results that this research shows, is the need for modelling penetration of a spudcan into a sloped seabed as the maximum moment does not have to occur in combination with the largest vertical load.

2.3. Structural

This section will discuss various modelling methods to capture relevant behaviour mechanisms. Firstly, different structural modelling methods will be discussed by explaining the theory behind the models and existing literature on these models. Secondly different soil modelling methods are obtained from literature and compared to accurately model soil spudcan interaction.

2.3.1. Structural modelling

The basis for structural modelling starts with the need to describe the response of a structure under loads. This is done by using Euler-Bernoulli beam theory, which gives a differential equation to describe the behaviour of a beam. But a structure is usually comprised of multiple beams, which creates the need for a system that can calculate the response of many beams, this modelling method is Finite Element (FE) modelling.

Euler-Bernoulli beam theory

Euler-Bernoulli beam theory is a theory describing the load carrying and deflection behaviour of beams. This beam theory applies linear elastic theory and ignores shear and rotational inertia effects.
Another important property of the Euler-Bernoulli beam is that taking successive derivatives of the deflection will lead to relevant equations. Starting with the equation for slope (θ) which is the first derivative of displacement (2.49). This holds true due to the linearization which assumes small displacements and rotations.

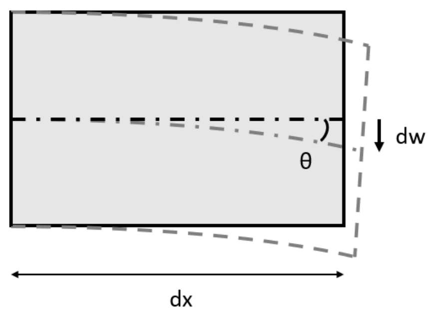

Figure 2.25: Determination of slope in a beam element

The second derivative is equal to the moment when multiplied with elastic modulus (E) and second moment of inertia (I) (2.50). The third derivative of displacement is shear (2.51). The fourth derivative is equal to the distributed load (2.52) and describes the equilibrium position of a beam.

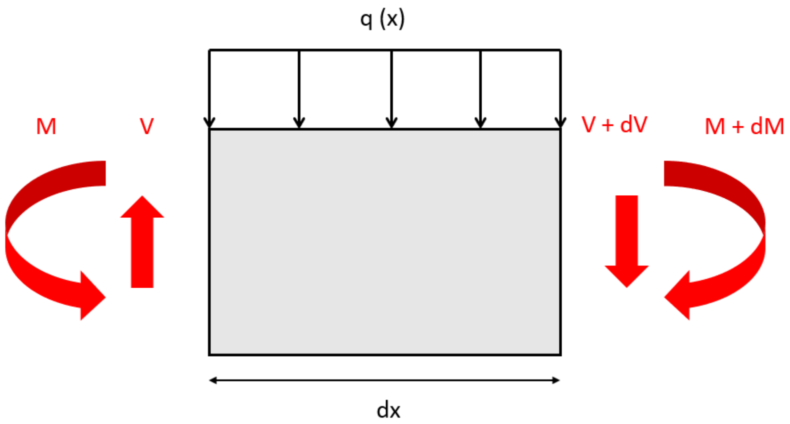

Figure 2.26: Free body diagram of beam element

$$\frac{dw}{dx} = \theta \tag{2.49}$$

$$EI\frac{d^2w}{dx^2} = M \tag{2.50}$$

$$EI\frac{d^3w}{dx^3} = V \tag{2.51}$$

$$EI\frac{d^4w}{dx^4} = q \tag{2.52}$$

These are the basic formula's for describing load carrying and deflection behaviour in an equilibrium position. But when the dynamics of a beam need to be determined an extra term is added to the equation (2.53). The derivation can be done by determining the energy in the system and applying Lagrangian method to get to the Euler-Lagrange equation for a beam.

$$EI\frac{d^4w}{dx^4} + \rho A\frac{d^2w}{dt^2} = q \tag{2.53}$$

where:

E	is the Young's Modulus
I	is the second moment of inertia
ρ	is the material density
A	is the cross-sectional area

Where *w* is the deflection of the beam in the z-direction at a chosen point along the length of a beam, *q* is the distributed load on the beam. Also *E*, *I*, ρ, *A* are the elastic modulus, second moment of inertia, material density and cross-sectional area respectively.

Finite element modelling

This section will explain the basics of finite element (FE) modelling. The FE method is a crucial tool in analyzing behaviour of systems and especially complex systems. This modelling method is employed in numerical simulations to gain insights into responses of systems. There are four basic steps when doing a numerical FE calculation.

- Discretize geometry
- Define shape function
- Compute elemental matrices
- Assemble global matrices

The first step is based on the essential fact of finite element modelling that a large structure of which the behaviour needs to be analysed is divided into smaller pieces called elements. Each element has 2 nodes, one at each end of the element and is also the connection piece between elements. Each element can be seen as a spring for which the parameters can be selected. For modelling beams the parameters are flexural stiffness (EI) and axial stiffness (EA). So to complete the first step all nodes and elements that describe a structure must be defined.

The second step is to define the shape functions, which are also referred to as interpolation functions. The interpolation functions describe the variation of physical quantities such as displacements within an element as a function of spatial coordinates. These functions allow for the approximation of physical behaviour across the element and facilitate the expression of field variables in terms of nodal values.

The third step is computing the elemental matrices, which is an important step into breaking down a complex problem into smaller manageable elements and formulate an approximation of the solution. This is achieved by computing a matrix for each element called elemental matrices. These matrices contain stiffness and mass distribution information in the element in the form of partial differential equations (PDEs) which are approximated by the shape functions and basic physical functions. These functions serve as weighting factors to express the PDE in nodal values which can be applied in matrix form. In the application of structural dynamics the stiffness matrix of an element covers the local behaviour of applied forces and nodal displacements.

Once these PDEs have been assembled the weak form must be formulated, which is a formulation that emphasizes the minimization of potential energy within the element. This is done in 3 steps [24]:

1. Multiply governing PDE with a weight function (w) and integrate over an element.
2. Apply integration by parts to separate differentiation of w and u.
3. Identify primary and secondary variables, where primary variables relates to essential (geometric) boundary conditions and secondary variables to natural (force) boundary conditions.

The assumption is made that all boundary conditions are natural, leading to the formulation of internal forces being included in the weak form. This assumption simplifies the formulation by treating all conditions as force-related, allowing for a comprehensive integration of internal forces into the weak form. Applying this FE theory to 2D case, the stiffness matrix of an element can be determined for a case with 3 DOF, 2 translation and 1 rotation, by a 6x6 matrix. The size is determined as an element consists of 2 nodes which both have 3 DOF each, causing the need for a 6x6 matrix.

$$k_{local} = \begin{bmatrix} \frac{AE}{L} & 0 & 0 & \frac{-AE}{L} & 0 & 0 \\ 0 & \frac{12EI}{L^3} & \frac{6EI}{L^2} & 0 & \frac{-12EI}{L^3} & \frac{6EI}{L^2} \\ 0 & \frac{6EI}{L^2} & \frac{4EI}{L} & 0 & \frac{-6EI}{L^2} & \frac{2EI}{L} \\ \frac{AE}{L} & 0 & 0 & \frac{-AE}{L} & 0 & 0 \\ 0 & \frac{-12EI}{L^3} & \frac{-6EI}{L^2} & 0 & \frac{12EI}{L^3} & \frac{-6EI}{L^2} \\ 0 & \frac{6EI}{L^2} & \frac{2EI}{L} & 0 & \frac{-6EI}{L^2} & \frac{4EI}{L} \end{bmatrix} \tag{2.54}$$

The global stiffness is then determined by assembling local stiffness matrices to construct a global stiffness matrix of size $n\,x\,n$ where n is equal to the number of nodes in the mesh times the amount of DOF included in the model.

Structural models of JU's

This section dives into previously implemented modelling methods for creating a structure representing a JU. An overview of model types can be divided in 2D and 3D cases.
Initially researchers were busy with modelling 3 legged JU's for which preload is applied per leg, which meant that the governing leg could be analyzed if a side view was taken from the structure. This justifies the use of a 2D model for a 3D structure. Furthermore the model is made-up of equivalent beams for the truss legs, where instead of a complex truss structure is modelled, one beam is modelled with parameters that are equivalent to the complex structure, see 2.27. Previous research on modelling foundations for JU on sand has applied an equivalent 2D structural model for a JU on sand during operation under wave loading [8]. Here the complex JU is modelled as equivalent beams which have equivalent properties for the legs and hull.

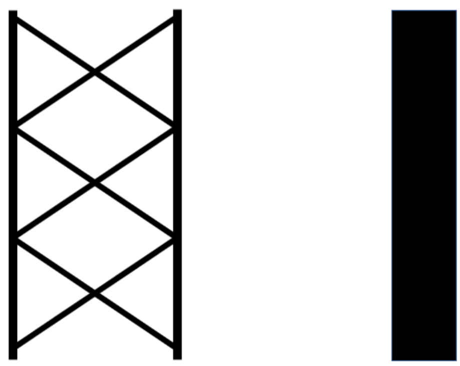

Figure 2.27: Truss leg (left) and equivalent leg (right)

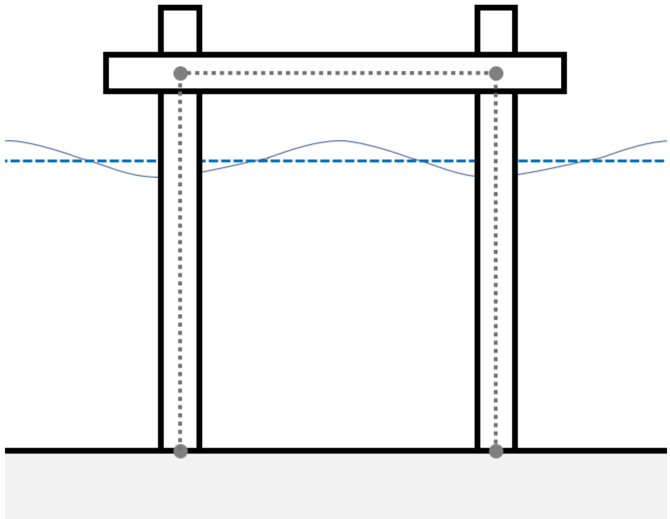

Figure 2.28: Equivalent 2D model of a JU on a seabed in waves.

These models are good for global analysis and are relatively quick to set-up and calculate with. This is because the amount of elements is reduced when comparing it to a more complex model.
The second method for modelling global response of JU's is 3D modelling. Same as in the 2 dimensional case, the legs and hull are modelled as equivalent beams each with corresponding parameters for stiffness and geometry. However now loads can be modelled at individual legs and a more global response can be sketched.Traditionally most JU's are 3 legged [17] but for the wind industry a 4 legged vessel is used [28] and has not been researched as abundantly as the 3 legged version.

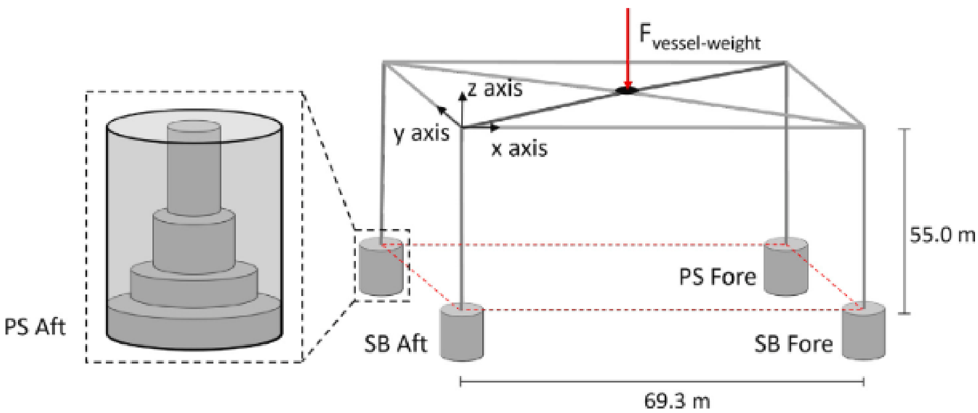

Figure 2.29: Equivalent 3D model of a JU on a seabed [28]

Leg-hull interface

The interface between the legs and the hull is a very critical component as loads are transferred from the leg into the hull. Also these interface contain pinions which drive the legs up and down and are driven by motors connected to gearboxes, see Figure 2.30. These interfaces can be modelled as simple rigid connections for displacements and rotations ([22], [1], [8]) or they can be modelled as springs and gap elements to capture more realistic behaviour of the load distribution [35]. Where according to literature, the horizontal stiffness of the jacking system has a great influence on the load distribution and shows an unequal loading of the pinions [35].

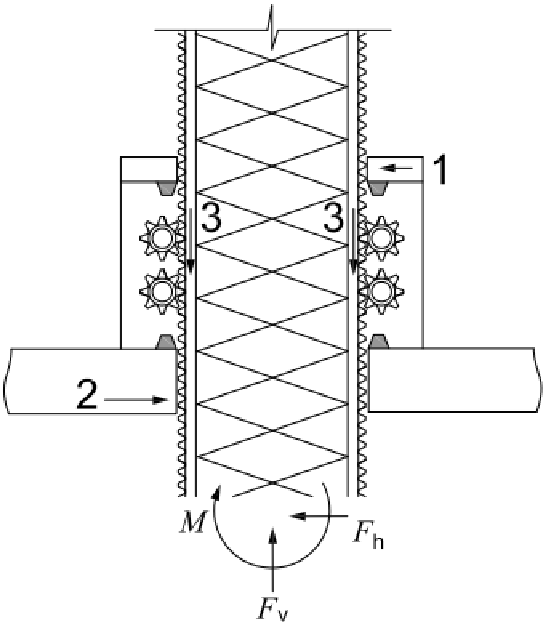

Figure 2.30: Representative leg-hull interface [21]

The loads that occur at the seabed travel up the leg and into the interface as F_v, F_h, and M. The upper (1) and lower (2) guide as can be seen in 2.30 will cause a reaction couple to cause moment equilibrium along with the couple occurring in the pinions (3).

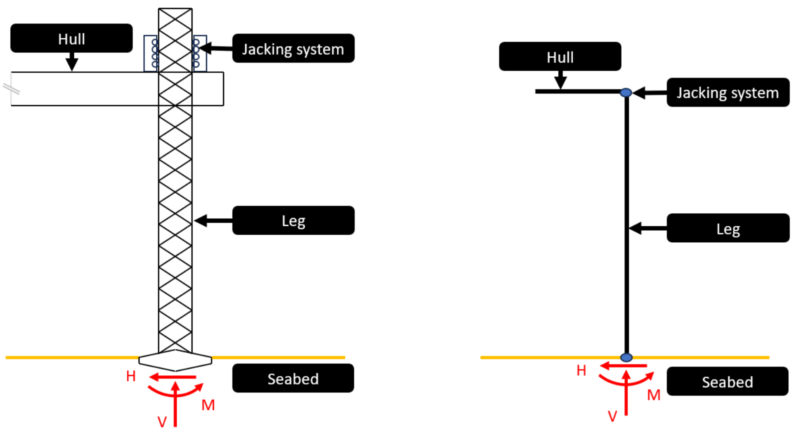

Figure 2.31: Equivalent leg-hull interface

Implementing assumptions for leg-hull interface, an equivalent model can be created where the jacking system is modelled as a rigid node as can be seen in Figure 2.31. For this model the moment induced at the seabed along with horizontal and vertical loads will be transferred through the rigid connection to the hull.

Geometric non-linearity

Geometric non-linearity occurs when large deformations do. This is due to the stiffness of an element changing with the displacement. In linear systems the stiffness matrix is calculated once at the beginning but here the stiffness is dependent on the displacement of the element, which varies per calculation step. This can be solved using an iterative method where an initial displacement is chosen, then based on that displacement a mass and stiffness matrix are created. Then a new displacement is created and

for that displacement a new stiffness is determined. This repeats itself until the model is finished with running.
One example of this is the P-Δ effect where additional moments in the legs are created due to load eccentricities occurring due to displacement. To take this effect into account it's contribution must be determined and the structural model must be able to handle this non-linearity.

2.3.2. Sensoring

For determining the loads in a JU measuring devices must be applied to give more insight into structural limits and when they are approached. Typically, there a 2 measurements being made on vessels during operations which are leg loads and Rack Phase Difference (RPD). The first sensoring method in use is leg load which is determined through measurement of the current in the motors of the jacking system. By measuring the currents in the motors, the resistance of the motor is equal to the torque delivered by the motor and can be expressed by force times arm. This force per motor is then summed per chord and per leg to determine total leg load in vertical direction. This system is called the Variable Speed Drive Rack and Pinion Drive System and is a patented GustoMSC system.
The second sensoring method is RPD, which is used to measure the bending of the leg. This is done by measuring the extension of each leg chord during operation and subtracting the smallest value for extension by the largest, yielding the difference in rack phase, see Figure 2.32. Research shows how RPD is present when a spudcan is eccentrically loaded due to an uneven hard sand seabed [29]. This indicates that RPD is a good measurement tool for determining the effect of seabed slope.

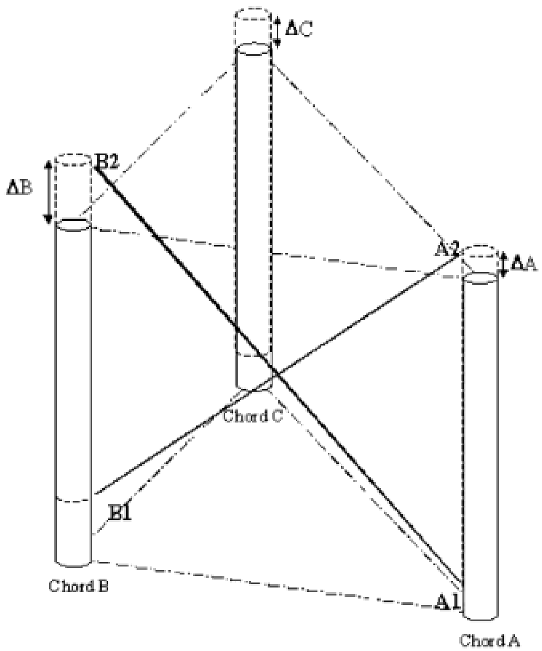

Figure 2.32: Rack Phase Difference in a truss leg [29]

Another sensoring method which is currently not applied on a JU, is a measuring device in the upper and lower leg guides to capture the behaviour and extent of leg bending. A patent has been Published by GustoMSC for a device which would be able to perform this measurement [2]. The goal of this device is to measure a parameter which can be vertical load or horizontal load of leg onto leg guide, angle, speed or acceleration of leg to or onto leg guide. The principle goal here of this sensoring method is to give a more accurate description of the leg bending occurring during JU operations.

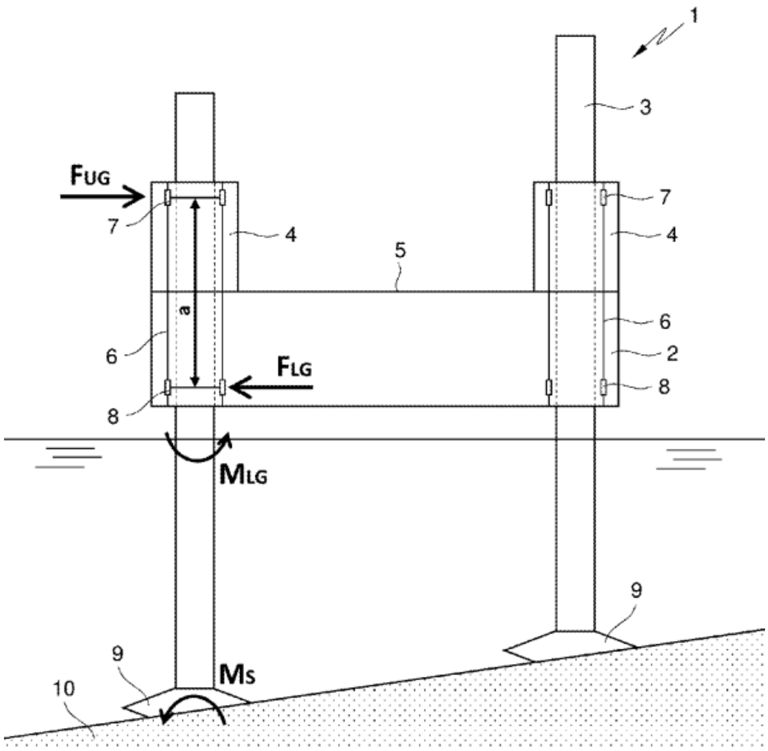

Figure 2.33: Simplified hull showcasing location and loads to be measured by patent [2]

The relevance here comes when the simplified hull is compared to the assumption for an equivalent leg-hull interface where the lower guide moment will be fully transferred through from leg to hull via one node. This shows that determining the moment in an equivalent JU model is of utmost relevance and is comparable to the lower guide moment.

3 Modelling

This chapter describes the steps taken according to the framework in order to initialize models for geotechnical and structural applications for describing a spudcan on a sloped seabed and JU during preloading respectively. Initially the framework is described followed by the sections on geotechnical and structural modelling.

3.1. Framework

This chapter entails the combination of geotechnical and structural domains by means of a framework in order to describe a JU during preloading on a sloped seabed. In order to visualize the steps taken in the framework a flowchart is created showing the relation between the geotechnical and structural model which is found in Appendix B.
The geometry of the 4 legged JU is defined where one leg is positioned above a sloped seabed, which is then cut out of the structural model and modeled using the geotechnical model, the location of the cut is referred to as the interface. For the remaining 3 legged structural model, a set of stiffness values is determined, describing uniaxial stiffness response of the remaining hull, legs and soil stiffness configuration (Appendix B).

This equivalent stiffness along with the sloped leg geometry are then used as an input to define the geotechnical model geometry, where the soil domain is also defined as can be seen in Figure 3.1. After the soil and structure dimensions are integrated into the Plaxis3D model, the preloading process is applied, where a vertical load representing a discrete step of the preloading process is applied at the top of the leg. When calculations are complete, the reaction loads at the interface are obtained and put back into the structural model as an input. The foundation stiffness is calculated using the Plaxis3D model but in a different configuration, 2 cases are run to calculate foundation stiffness values; one for a sloped seabed and one for a flat seabed. Nevertheless, the reaction loads are re-applied in the structural model at the interface and the foundation stiffness values at the footing nodes of all the remaining legs on a flat seabed.

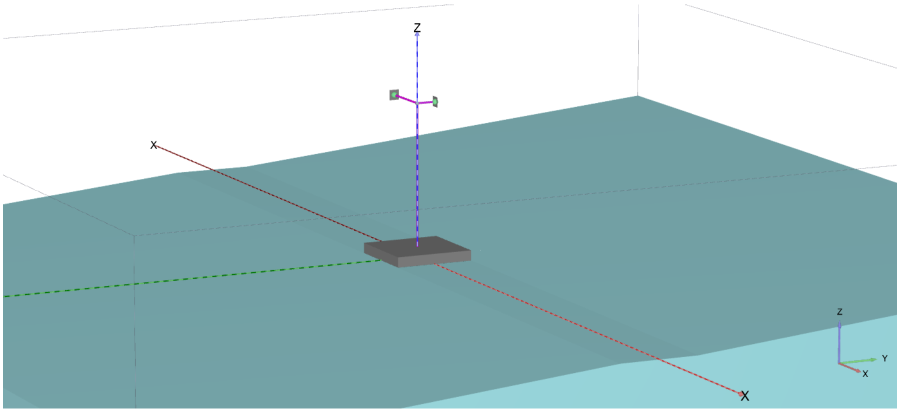

Figure 3.1: Geotechnical model overview for calculating reaction loads

With the structural model complete, the system can be solved and results are obtained in the form of displacements of the leg-hull interface nodes along with the corresponding reaction forces and moments. These forces and moments are then used to describe load distribution effects due to seabed slope interaction effects.

3.1.1. Preloading process

This section describes the application of loads on the structure in order to model a preloading process and to obtain all load displacement behaviours. This preloading is then modelled by increasing and decreasing a vertical load on the rigid footing according to a preloading procedure. This preload procedure describes the vertical load shifting from one LP to the other. At jacking phase, the weight load is assumed to be perfectly distributed over all 4 legs, and as preloading starts, the vertical load from one LP is transferred to the other.
The preloading procedure is modelled for the two LP's, as during preloading, one LP is loaded while the other is unloaded. For the first LP, the vertical load starts at 0 MN and increases up to jacking load. For the second phase the vertical load is increased to maximum preload, afterwards in phase 3 unloaded and finally brought back up to operational load.

Table 3.1: Preloading phases

Table 3.2: Phases LP 1

Phase	Load	Unit
1.1 - Jacking	125	MN
1.2 - Preload	216	MN
1.3 - Unload	34	MN
1.4 - Operation	125	MN

Table 3.3: Phases LP 2

Phase	Load	Unit
2.1 - Jacking	125	MN
2.2 - Unload	34	MN
2.3 - Preload	216	MN
2.4 - Operation	125	MN

At the end of this procedure the soil underneath the spudcans has been preloaded such that lifting operations causing large shifts in vertical reaction loads in legs to occur.
The procedure in Plaxis is discritized to obtain reactions at steps between phases to more accurately describe the variation of stiffness during the preloading operation. For example to obtain the results between phase 1.1 and phase 1.2, an extra vertical load step is added ($V = 170.5MN$) to obtain behaviour in the transition between phases. The full preloading process with all steps included can be found in Appendix B.
These vertical steps are then implemented on both soil-structure interaction models, one model for calculating the reaction loads and moments at the leg-hull interface (Model 1) and another model for calculating foundation stiffness (Model 2). For Model 2, the value of the test loads (F_{test}, M_{test}) are chosen based on operational loads that occur in the field. The data is supplied from in-house sources and is set to $100MN$ and $100MNm$ for horizontal translation and rotation directions. For each direction ($u_x, u_y, \theta_x, \theta_y$) the load is applied in positive and negative direction. This is done to model the effects an asymmetrical seabed geometry could potentially give. An overview of the model is seen in Figure 3.3,

where the seabed is assumed to be flat and only the footing is activated for calculating foundation stiffness as can be seen by the grey beams and boundary conditions when compared to Figure 3.1. To obtain the stiffness during the preloading operation for a given LP, the applied load and resulting displacement of the footing are measured and plotted, with the slope of the plot being equal to the stiffness per step. Obtaining uniaxial stiffness' is done by implementing a set of 8 independent test phases which branch off of each vertical load phase. These 8 phases keep the vertical load constant, remove the stiffness of the leg and apply load in translational and rotational directions for the positive and negative horizontal axes (X & Y). After these test phases have been applied, the loading in vertical direction resumes, continuing on the history of the previous vertical step.

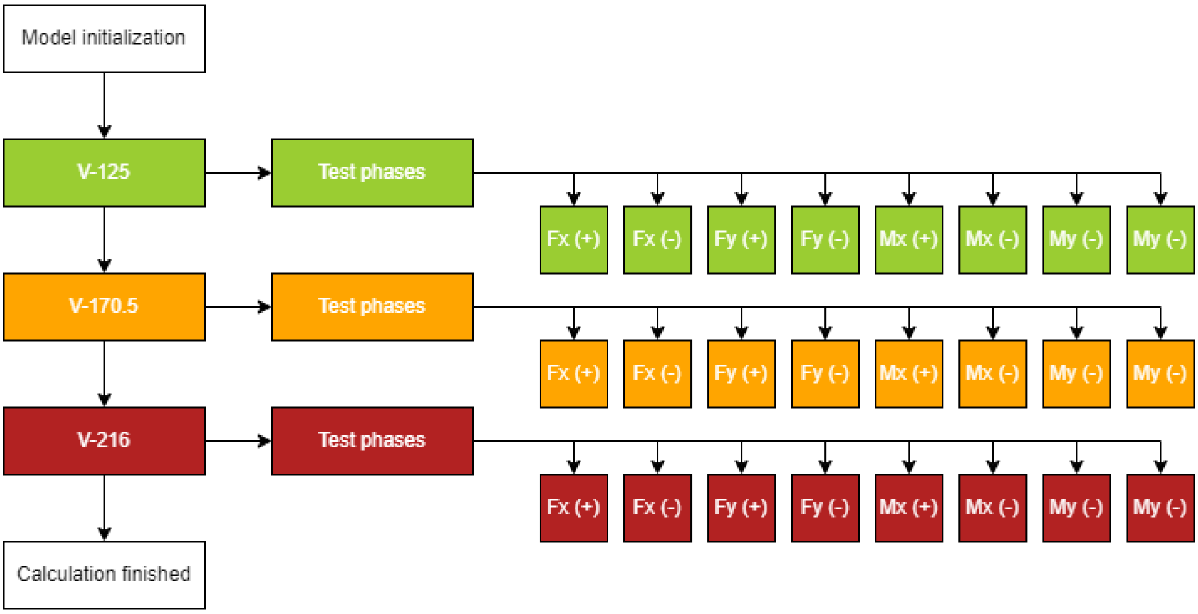

Figure 3.2: Overview of load steps for first 3 steps of LP 1

The load steps taken in the overview in Figure 3.2 are for LP 1 which goes from zero load at model initialization up to maximum preload ($V = 216\ MN$) with 2 steps in between for which foundation stiffness is determined.
In addition to determining foundation stiffness for a sloped seabed, the same procedure is implemented in a flat configuration as can be seen in Figure 3.3. The application of the described methodology will result in symmetric results for stiffness values in X- and Y-directions in translation and rotation, since the seabed is flat.

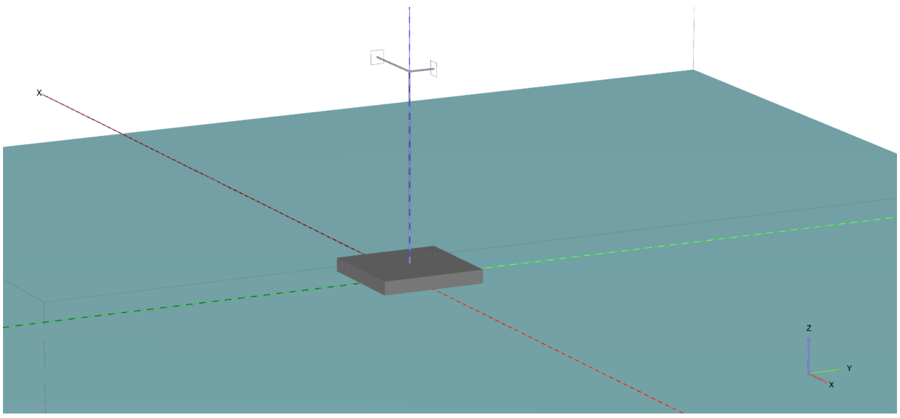

Figure 3.3: Geotechnical model overview for calculating foundation stiffness on flat seabed

3.2. Geotechnical model

This section will elaborate further on the choice of the geotechnical model used to model a spudcan penetrating a sloped seabed. The various steps taken to achieve this will be shortly described. Various modelling methods will be discussed in order to answer the research question. Followed by a further explanation of the selected modelling method. Afterwards, model parameters are defined consisting of soil constitutive model, dimensions, boundary conditions and load phases. Once the model is initialized, calculations are performed and results are obtained.

3.2.1. Soil-structure modelling methods

There are various ways to model a footing on a seabed, options range in complexity from a hand-calculation to a small strain finite element approach to a large deformation finite element method.
The most simple of these methods is the hand calculation, which is based on ISO code and other industry approved methods. This method is good for initial estimations and standard bearing capacity calculations for footings on flat surfaces. The drawbacks are that this method does not take soil hardening into account nor can it take the sloped seabed into account.
The next method that is considered is the small strain finite element approach (SSFE), which is characterized by its ability to model small deformations. This model works by meshing the geometry of the soil before calculations and does not allow for re-meshing during calculations. For implementing the SSFE, a software package such as Plaxis or OpenSees can be implemented. Both packages are able to account for various soil constitutive models, soil geometries and allow scripting through python to allow for quick iteration.
The most complex model that can be implemented is a large deformation finite element (LDFE) method which is able to re-mesh at every point in the calculation. This re-meshing leads to very accurate penetration calculations and more accurate mobilization of soil compared to SSFE. This re-meshing however does come at a cost of additional complexity and calculation time.
The chosen modelling method is the SSFE approach using Plaxis 3D. This is done as a footing on a sloped seabed can be modelled for small deformations. As an assumption is that slopes on sand will be considered, the deformation will be small relative to the size of the footing, so the choice is made to not implement the LDFE method.
Now that the modelling method is chosen, the steps that need to be taken to answer the sub-question need to be taken. The spudcan geometry must be described, an asymmetric seabed geometry must be defined, and a soil constitutive model needs to be chosen.

3.2.2. Soil constitutive model

Choosing the correct soil constitutive model is important when certain effects need to be taken into consideration. LE modelling is good for small strain problems, MC is accurate for initial guesses and uses little parameters but cannot model hardening. Finally HS model uses more parameters but is able to model hardening due to compression and shear.
For the application of soil-structure interaction during preloading process of a JU, the evolution of stiffness is of importance to take into account. This calls for the application of the HS model as this can model the stress dependent soil stiffness which can be translated to a global stress-dependent stiffness.
Soil parameters for the constitutive model are to be selected for a sand, as the goal is to model a low penetration in order to highlight seabed slope effects. The selected soil parameters are based on empirical formulas given relative density as input [5] and can be found in Appendix A.

Table 3.4: Soil parameters for HS model for various relative densities

RD [%]	γ_{unsat} $[kN/m^3]$	γ_{sat} $[kN/m^3]$	E_{50} $[kN/m^2]$	E_{oed} $[kN/m^2]$	E_{ur} $[kN/m^2]$	m [-]	ϕ [°]	ψ [°]
25	16,0	19,4	15000	15000	45000	0,622	31,1	1,1
50	17,0	19,8	30000	30000	90000	0,544	34,3	4,3
80	18,2	20,3	48000	48000	144000	0,450	38,0	8

As a SSFE model is selected for modelling soil-structure interaction, the strains in the model are assumed to remain small, in order to keep this assumption the soil with largest relative density is selected. This relative density is then selected as 80% (RD80) along with parameters describing strength and elasticity in Table 3.4.

3.2.3. Dimensions

This section explains the dimensions of the soil and structure geometries used in this research.

Structure dimensions

The spudcan is modelled as a square slab referred to as a square footing with footing length ($L_f = 15.5\ m$), width ($W_f = 15.5\ m$) and height ($H_f = 2\ m$) defined. The material model for the footing is selected as a rigid body, as the stiffness of the steel spudcan significantly larger than surrounding soil. To simulate the stiffness of the leg, a beam is attached to the footing with cross-section properties equal to the equivalent leg beam which is connected to a pair of rollers at the top to allow for vertical displacement but restrict translation in horizontal plane as well as rotation. Additionally an interface is included between the rigid body and soil volume, which represent an extra set of nodes to reduce local stiffness by a factor of 0.67 [6].

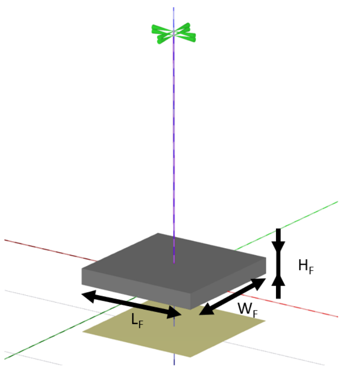

Figure 3.4: Overview of footing and leg including rollers and interface

Soil domain

The dimensions of the soil continuum are determined based on the size of the footing and especially on the area affected by the loading of the structure. The last point is especially relevant as the boundaries of the model are selected such that the boundary itself does not interfere with stress-strain behaviour of the soil continuum. The selected parameters for soil dimensions are length ($L_s = 200\ m$), width ($W_s = 200\ m$) and height ($H_s = 50\ m$), which can be seen in Figure 3.5.

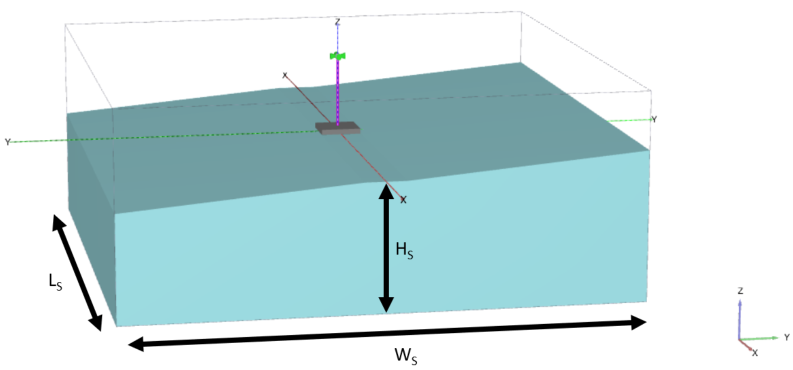

Figure 3.5: Plaxis 3D model overview

With the slope causing a height difference at the downhill (negative Y-direction) and uphill (positive Y-direction) with respect to the defined height (H_s). This height difference (H_Δ = 8.07 m) is determined using basic trigonometry for a slope (α) of 5 degrees.

$$H_\Delta = (\frac{W_s}{2} - \frac{W_f}{2})tan(\alpha) \tag{3.1}$$

3.2.4. Beam properties

The beam parameters of the equivalent leg are selected based on an equivalent JU model based on a GustoMSC designed NG-20000X JU.
Where A defines the axial area of the beam, I_2 and I_3 describe the moment of inertia about the 2^{nd} and 3^{rd} axes respectively and E describing the Young's modulus of the material. With the beam parameters being names according to local axis system for each beam as seen in Figure 3.6. Converting these local axes to a cartesian formulation, the second and third axes can be converted to y- and z-axis respectively.

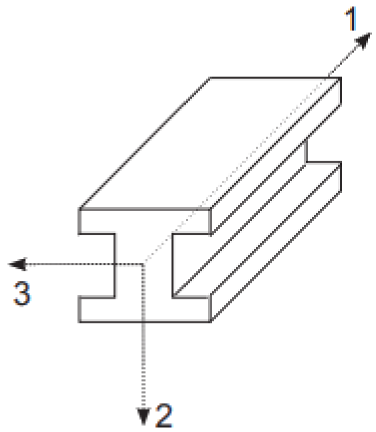

Figure 3.6: Local axis for beam element

The connection between leg and hull for the legs not on a slope are rigid in all DOF, a decision which is supported by research [8].

External stiffness

This section describes the methodology behind determining external stiffness of the JU vessel used in geotechnical calculations and can be found in Appendix B.

3.2.5. Calculation

In order to perform calculations using the soil continuum, a mesh is created using a mesh number defined in Plaxis, where a mesh number of 1 gives the coarsest mesh and deviates from most from the converged solution. By decreasing the mesh number a more refined mesh will be created which will lead to more convergent solutions leading to increased accuracy with the cost of an increased calculation time. The mesh selected for the calculation is chosen to be a factor 0.03.

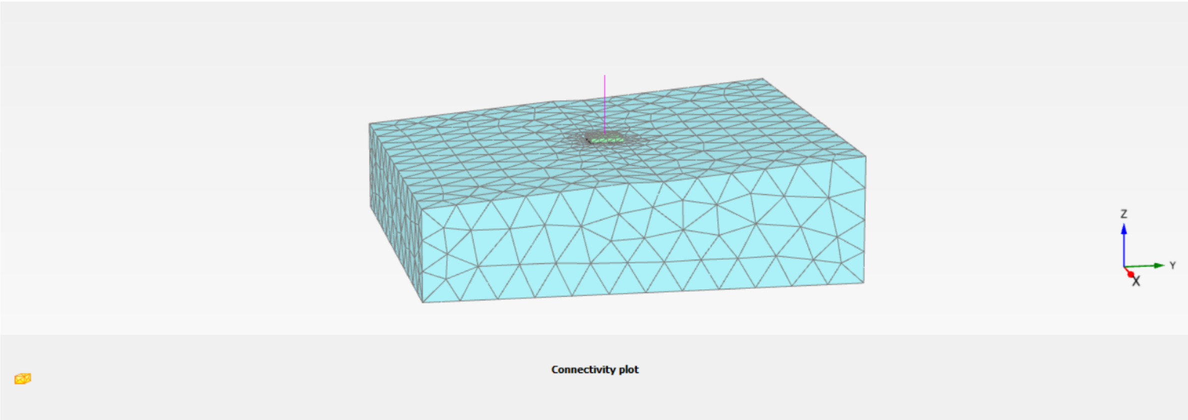

Figure 3.7: Plaxis 3D mesh overview

3.2.6. Obtaining results

The main goal in the prescribed geotechnical model is to describe non-linear soil-structure interaction during a preloading operation and the reaction such an operation causes in the form of reaction loads and moments. Obtaining the reaction loads is done by selecting the reaction loads at the top of the leg, which is referenced to as the interface node.

Additionally, a separate model per LP is created for determining the foundation stiffness per preloading step. Per vertical load step, a set of test loads is applied to the footing and the displacement in that direction is recorded. Now with these values a global stiffness value for each translation (X,Y,Z) and rotational (θ_X,θ_Y) direction are obtained by linearizing the stiffness results in positive and negative direction using the average as output.

First in determining stiffness the definition is defined as force over displacement or stress over strain. With a linear system, the stiffness is also linear and the slope will be constant.

$$K = \frac{F}{u} \tag{3.2}$$

But in a non-linear system the stiffness is dependent on the force or stress applied to the system at a given point. This leads to the need for a second definition of stiffness which states that the stiffness is equal to the slope between two points along the curve.

$$K = \frac{\Delta F}{\Delta u} \tag{3.3}$$

For this non-linear load-displacement behaviour 2 main types of stiffness are defined; secant and tangential stiffness.

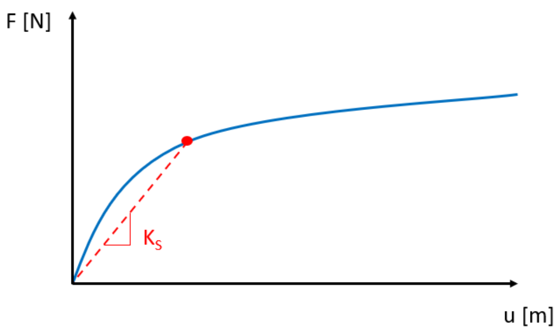

Figure 3.8: Secant stiffness of load displacement curve

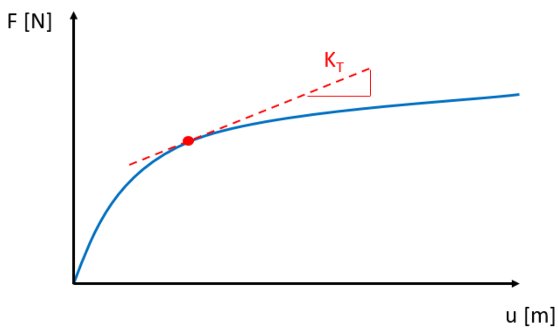

Figure 3.9: Tangential stiffness of load displacement curve

The secant stiffness displayed in Figure 3.8 is determined using formulation for stiffness in non-linear load-displacement curves Equation 3.3 but with the starting point equal to the origin. The stiffness

determined is thus a straight line between origin and the selected point of interest.
Tangential stiffness is the stiffness for a single point which can be determined for analytical solutions by means of a Taylor series. The Taylor expansion allows a function to be approximated by an infinite sum of the functions derivatives. Using this practically can be done in the form of finite difference equation by using neighbouring points relative to the selected point of interest along the load-displacement curve.
Now some background is given to determining stiffness values, the actual method for determining stiffness is done by taking the initial stiffness of each load-displacement or moment-rotation curve and averaging the values for positive and negative directions.

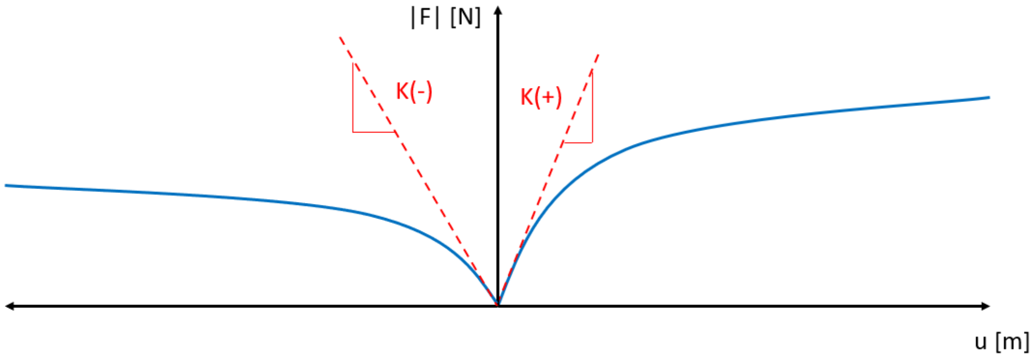

Figure 3.10: Linearization of load-displacement plots to determine slope

When the plot is considered as above, the vertical axis shows the absolute load values to highlight the asymmetry of load-displacement results. The initial stiffness is taken for both plots and are averaged to determine the final stiffness value.

$$K_{avg} = \frac{K_{(+)} + K_{(-)}}{2} \tag{3.4}$$

This stiffness value is averaged out in order to allow for description of foundation stiffness as a single spring in later modelling. This decision does however limit the effect of the asymmetric seabed geometry, where the averaging will cause displacements and rotations into and away from the slope to be underestimated and overestimated respectively. This can be said as displacement and rotation into slope direction are expected to result in a larger stiffness response than away from the slope.
These stiffness' can be translated into matrix for in order to be implemented into the structural model. The stiffness matrix that is created will be a diagonally populated matrix, and is unique for each vertical load step in the model.

$$\begin{bmatrix} F_x \\ F_y \\ F_z \\ M_x \\ M_y \\ M_z \end{bmatrix} = \begin{bmatrix} K_{xx} & K_{xy} & K_{xz} & K_{x\theta_x} & K_{x\theta_y} & K_{x\theta_z} \\ K_{yx} & K_{yy} & K_{yz} & K_{y\theta_x} & K_{y\theta_y} & K_{y\theta_z} \\ K_{zx} & K_{zy} & K_{zz} & K_{z\theta_x} & K_{z\theta_y} & K_{z\theta_z} \\ K_{\theta_x x} & K_{\theta_x y} & K_{\theta_x z} & K_{\theta_x\theta_x} & K_{\theta_x\theta_y} & K_{\theta_x\theta_z} \\ K_{\theta_y x} & K_{\theta_y y} & K_{\theta_y z} & K_{\theta_y\theta_x} & K_{\theta_y\theta_y} & K_{\theta_y\theta_z} \\ K_{\theta_z x} & K_{\theta_z y} & K_{\theta_z z} & K_{\theta_z\theta_x} & K_{\theta_z\theta_y} & K_{\theta_z\theta_z} \end{bmatrix} * \begin{bmatrix} u_x \\ u_y \\ u_z \\ \theta_x \\ \theta_y \\ \theta_z \end{bmatrix} \tag{3.5}$$

However an assumption is made that there is no coupling between the various directions. In reality this is not true as off diagonal terms point to coupling between force and displacements in different directions. With this new assumption the matrix in 3.5.

$$\begin{bmatrix} F_x \\ F_y \\ F_z \\ M_x \\ M_y \\ M_z \end{bmatrix} = \begin{bmatrix} K_{xx} & 0 & 0 & 0 & 0 & 0 \\ 0 & K_{yy} & 0 & 0 & 0 & 0 \\ 0 & 0 & K_{zz} & 0 & 0 & 0 \\ 0 & 0 & 0 & K_{\theta_x\theta_x} & 0 & 0 \\ 0 & 0 & 0 & 0 & K_{\theta_y\theta_y} & 0 \\ 0 & 0 & 0 & 0 & 0 & K_{\theta_z\theta_z} \end{bmatrix} * \begin{bmatrix} u_x \\ u_y \\ u_z \\ \theta_x \\ \theta_y \\ \theta_z \end{bmatrix} \tag{3.6}$$

3.3. Structural model

This section will dive into the selection of a suitable structural model in order to answer the research question. The choice of structural approach for modelling a JU is highlighted along with model parameters and boundary conditions. The structural model has as goal to capture the load distribution throughout the JU during preloading procedure on a sloped seabed.

3.3.1. Modelling methods

There are 2 main methods considered for modelling the global structural behaviour of a JU during preloading; full Plaxis 3D model and quasi-static FE model.
The full Plaxis 3D method allows the geometry to be described in Plaxis 3D as beam elements with CS properties equal to an equivalent JU. This method is most straightforward where the structural model also doubles as the geotechnical model, but the drawback here is that load-enforced leg extension mechanism needs to be implemented in order to control leg load. This load-enforced leg-extension mechanism is complex if not impossible to integrate into Plaxis 3D as it's functionalities as a structural FE solver are limited.
The second method implements a structural FE solver using Python where as with the first method an equivalent JU is modelled by inputting nodal coordinates and beam elements with according CS properties. Here potential soil-structure interaction effects can simply be implemented as boundary conditions at the footing nodes and no leg-extension mechanism needs to be implemented. Another perk of this method is the de-coupling of geotechnical and structural programs, as these programs can be developed and adapted separately, saving on computational time and allowing interchangeability of the two components as long as the interface between the methods remains constant.

3.3.2. Modelling steps

The first step is to initialize the model by selecting the dimensions and mechanical properties of the JU's hull and legs. The dimensions and mechanical properties are based on the NG-20000X JU.
The second step is to identify the leg positioned on a sloped seabed and to cut this model at the leg-hull interface and simulate the model in a soil-structure interaction model. Afterwards the foundation stiffness values for the remaining legs must be calculated and applied at the footing nodes.
The third step is to solve the quasi-static system for the given step in the preloading phase. The model will iterate with the same amount of output points from the Plaxis 3D results. The solved system will then give the results in the form of displacement of the JU and loads and moment at leg-hull interface.

3.3.3. Dimensions

The dimensions for a JU are according to the geometry of the GustoMSC designed NG-20000X, which has a hull length of $151\,m$, hull width of $58\,m$ and draft of $7.9\,m$. The legs have an overall leg length of $120\,m$ and can extend $86\,m$ underneath the hull [19].

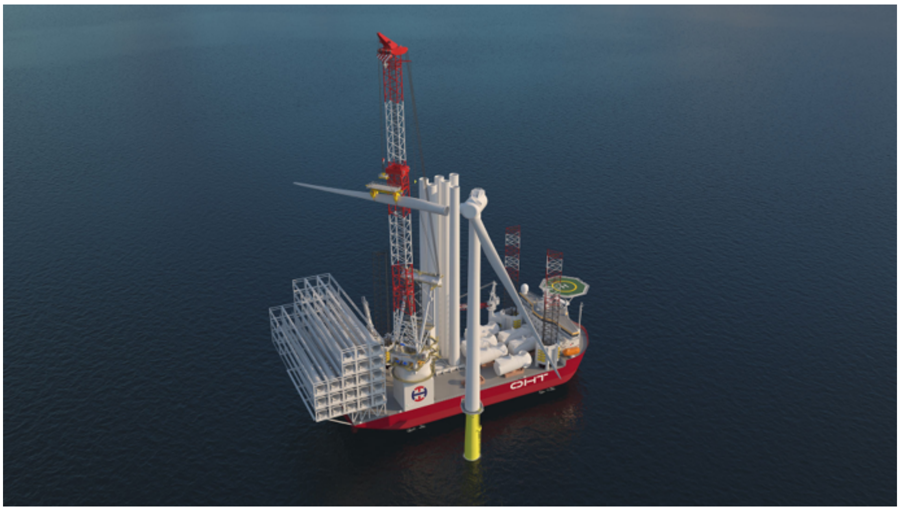

Figure 3.11: Render of a NG-20000X installing a wind turbine [20]

In order to model a simplified JU structure, a table-top model is created of all 4 legs and the distances between them. The lateral (L) and transversal (W) distances between the legs and the leg length (H) are defined in Appendix B and visualized in Figure 3.12.

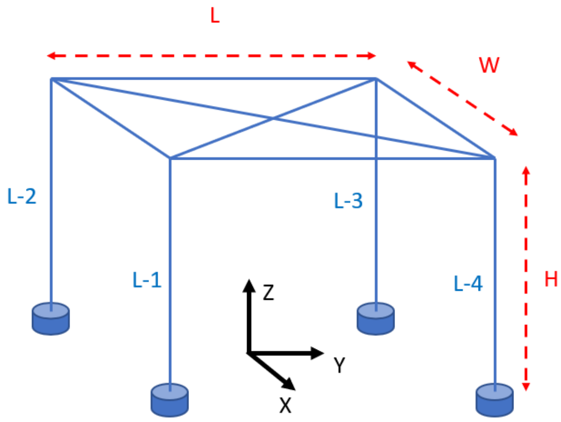

Figure 3.12: Dimensions for structural model of JU

3.3.4. Section & Material

The properties of the JU legs are captured by assigning properties to the cross-sections of the respective elements. As in reality a JU leg consists of 3 chords with X-braces, but they can be simplified by creating an equivalent beam with adjusted properties. The following properties are values based on a NG-20000X JU.

3.3.5. Determining equivalent stiffness

Implementing the substructuring approach, the interaction effect of the remaining vessel are taken into account by implementing a set of uniaxial equivalent springs in the geotechnical model. In order to determine these values, a set of load-displacement calculations are applied to the interface node, where a load or moment is applied in a specific direction and the displacement in that respective direction is measured. Using stiffness relation defined in Equation 3.2, the equivalent stiffness can be determined of the combined system of hull, legs and foundation stiffness values. To take an example, the stiffness in global Y-direction is to be considered where an equivalent load is applied ($F_{eq,Y}$), since a linear structural model is implemented, the sign of the applied equivalent load is irrelevant. Running calculations will give a displacement field of all nodes in the structural model, including the displacement of node 5

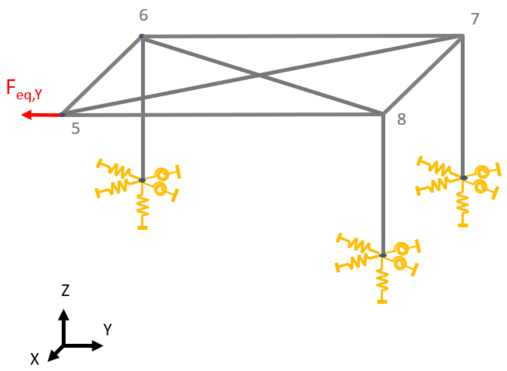

Figure 3.13: Overview of equivalent stiffness determination of hull, legs and foundation stiffness

in Figure 3.13 in global Y-direction. With the equivalent load and displacement known, the equivalent axial stiffness can be determined.
One limitation of this methodology is that with the application of a load in one direction, due to the asymmetry of the structure, the interface node will also displace in additional directions such as global X and Z-directions.

3.3.6. Boundary Condition

In order to hold the model to the seabed, a set of boundary conditions are applied to the model. In this case the spudcans are constrained by a set of 6 uniaxial springs at the end of each leg in Figure 3.12 which are attached to the fixed environment. The values for the springs are applied to simulate the variation of soil stiffness during preloading, this is done by updating the local spring stiffness at the spudcan nodes.

3.3.7. Solver

With the geometry of the equivalent JU implemented and geometry is meshed, a stiffness matrix can be assembled. The system is solved by means of matrix multiplication of the global stiffness matrix with the global global load matrix.

$$u = \mathbf{F} * \mathbf{K}^{-1} \tag{3.7}$$

3.3.8. Obtaining results

The results obtained for the structural model come in the form of a moment line and displacement plot to give an overview of the global response of the structure. Additionally the moments in the nodes representing the leg-hull interface are recorded and plotted to show their evolution during the preloading process, as these moments represent the lower guide moment. Supporting figures can be found in Appendix B

4 Results

This section will contain the results for geotechnical modelling, starting with soil testing to validate soil constitutive model behaviour. Secondly a calculation for soil stiffness will be conducted implementing industry standard methods according to [21]. Thirdly the equivalent hull stiffness is calculated to incorporate hull interaction into the geotechnical model. Followed by the results obtained from running the geotechnical model in the form of reaction loads and foundation stiffness values. Finally the results will be compared to industry standards to validate and verify the obtained results and methodology.

4.1. Soil-testing

In order to describe a proper soil-structure interaction, a soil constitutive model must be selected in combination with a soil type. In order to validate the selected soil, tests must be run on the soil sample to review its behaviour under certain types of loading. In the field, soil samples are taken from the location of operation and tests are run on the sample. The goal here is to test the soil sample in order to predict the behaviour of a structure on a larger scale.
In the application of this research a virtual soil test is performed in order to compare various soil constitutive models. The constitutive soil models under consideration are Linear Elastic (LE), Mohr-Coulomb (MC) and Hardening Soil (HS).

Table 4.1: Constitutive soil parameters - LE

E_{ref} $[kN/m^2]$	ν $[-]$
35660	0.3

Table 4.2: Constitutive soil parameters - MC

E_{ref} $[kN/m^2]$	v $[-]$	ϕ $[°]$	ψ $[°]$	c $[kN/m^2]$
35660	0.3	38	8	0

Table 4.3: Constitutive soil parameters - HS

E_{50} $[kN/m^2]$	E_{oed} $[kN/m^2]$	E_{ur} $[kN/m^2]$	v $[-]$	ϕ $[°]$	ψ $[°]$	c $[kN/m^2]$	m $[-]$
48000	48000	144000	0.3	38	8	0	0.45

The set-up of the soil test is represented as a cylindrical sample in an set-up where axial load (σ_{yy}) is applied from the top of the sample and a passive pressure (σ_{xx}) is applied by the fluid medium.

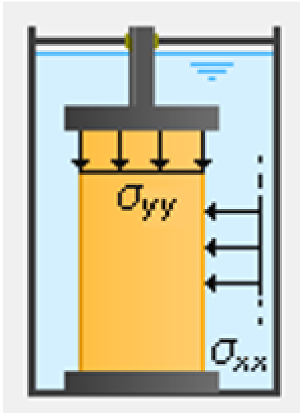

Figure 4.1: Triaxial test setup with load shown in 1st and 3rd principal directions

For each of these constitutive models, 3 plots are made to compare the models with each other on various aspects. The first is Mohr-Coulomb failure criterion to determine at what load combination the soil sample will fail. Here the expected results are that the MC and HS models will fail at the same load combination as the strength in both constitutive models are determined in the same way. The LE model is kept out of consideration as a purely linear model will never fail, and thus results would lie above the failure line for sand with an internal friction angle of 38°.

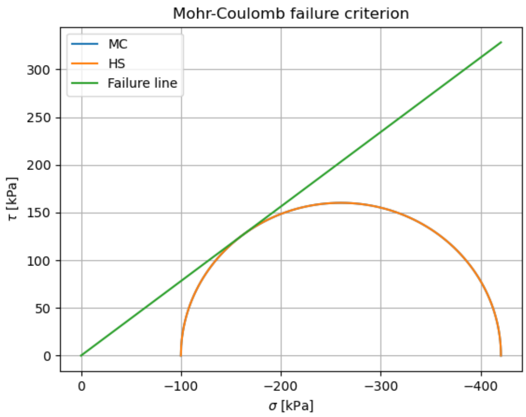

Figure 4.2: Mohr-Coulomb failure criterion for sand of 38°

The second plot is the axial stress-strain curve where the x-axis represents strain in axial direction in meters and the y-axis represents the stress in the axial direction in kPa. The LE model shows a straight line which is to be expected as the stress-strain behaviour stays constant in a linear situation. For a MC model the initial response follows the linear case up until above 400 kPa where a perfect plastic failure is displayed. Finally looking at HS model, the response initially increases in stiffness up to about 300 kPa and then a gradual decrease is seen up until the same height as in the MC model. This effect shown in the plot by the HS model is hardening, where intially more soil gets mobilized causing an increase in stiffness of the soil, with increased loading however the slope will decrease until failure occurs.

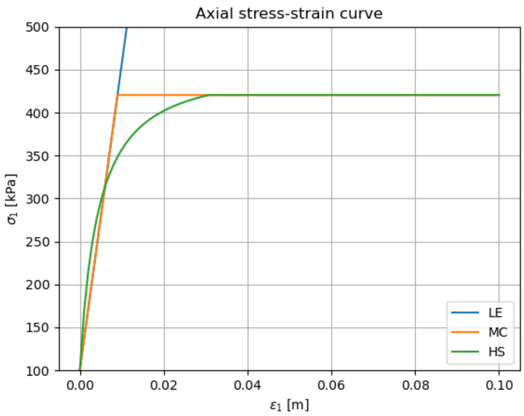

Figure 4.3: Axial stress-strain curve for sand of 38°

The third plot displays the relation between volumetric and axial strain during increased axial loading. The main effect displayed is dilatancy where initially as the axial strain on the x-axis increases, the volumetric strain decreases, but as axial strain increases, the volumtric strain will reverse which is caused by dilatancy in the soil.

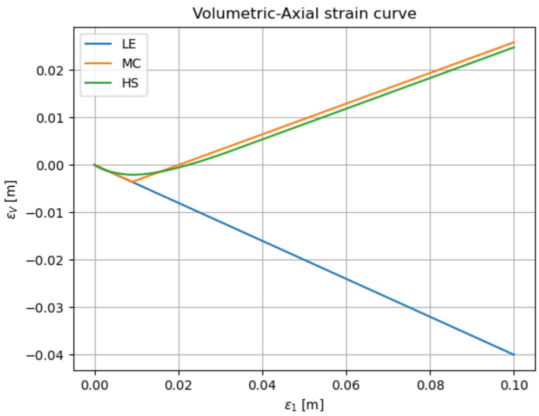

Figure 4.4: Volumetric-Axial strain curve for sand of 38° and dilation angle of 8°

By observing the behaviour of a soil sample in a soil test, a better understanding of local soil behaviour is obtained for various soil constitutive models.

4.2. Industry Standards

In order to set a baseline for stiffness values, the ISO guidelines are followed in order to calculate stiffness values at various steps during the preloading process. These ISO stiffness values are based on purely uniaxial loading conditions. The formulas for ISO stiffness can be found in 2.46, 2.47, 2.48. Additionally the shear modulus of soil must be determined which is based on soil parameters also used in Plaxis model. The only input for these ISO stiffness formulations which defines strength is the shear modulus: *G*. Obtaining the shear modulus (G) is done by lab testing of soil samples but with the absence of lab tests, shear modulus can be determined by implementing a simple formula relating the shear to elasticity modulus (*E*) and Poisson's ratio (ν).

$$G = \frac{E}{2(1+\nu)} \tag{4.1}$$

For the selected soil parameters describing soils according to [5] with relative densities for sand of 25%, 60% and 80%. For each soil type, the Poisson's ratio is kept constant ($\nu = 0.3$), along with the geometric input 4.2.

$$B = \sqrt{\frac{4 * A}{\pi}} = 17.5m \tag{4.2}$$

The equivalent diameter is calculated using the area of the square footing in order to properly implement the square shape for the ISO formula which is based on a circular footing.

Table 4.4: Soil stiffness for circular foundation on isotropic elastic medium according to ISO 19905-1.

D_R [%]	E $[MN/m^2]$	G $[MN/m^2]$	K_V $[MN/m]$	K_H $[MN/m]$	K_R $[MNm/°]$
25	45	17.31	864.9	737.0	769.6
60	90	34.61	1729.8	1474.1	1539.2
80	144	55.38	2767.6	2358.5	2462.7

These stiffness values are thus calculated using ISO standard calculations for a circular footing on a isotropic elastic soil for small strain loads. The method however does not include any hardening effects of a HS model, but nonetheless can give valuable insight into comparison of results by means of order of magnitude.

4.3. Equivalent hull stiffness

Here the sloped leg is cut out of the structural FE model and test loads are applied to the interface to determine the displacements and in turn calculate the equivalent stiffness in X, Y directions for translation and rotation equating to 4 springs stiffness values. These values can then be described in Plaxis by implementing formulas for length (L) and area (A) of equivalent beam in combination with a set of boundary conditions. The values used to determine the equivalent hull stiffness along with figures and graphs can be found in Appendix B.
The results show a insignificant difference between the displacement in the Python and Plaxis3D models, all below 1%. The differences in Python are smaller than the displacements in Python which could be explained by the fact that in the equivalent stiffness determination in Python, the asymmetric model causes a displacement in a direction other than the direction of forcing. However since this difference is so small, the effect of this off-diagonal displacement is neglected and no further investigation is done to determine exact causes.

4.4. Plaxis 3D geotechnical simulation

This section will report on the obtained results from the geotechnical phase in the framework by displaying load-displacement results and show the calculated stiffness' and reaction loads which are implemented by the structural model. A separate geotechnical model is created for each LP, as the vertical load path differs between footings on opposite LP's but equal along the same LP. Additionally the first load-unload for LP1 and LP2 are simulated for load-displacement plots as to avoid crowded graphs.

4.4.1. Load displacement

The geotechnical model is assumed to be a square flat footing with a beam representing the leg and its stiffness properties above the footing. The bottom of the footing is in complete contact with the seabed and the slope goes uphill in the positive Y-direction and downhill in the negative Y-direction.

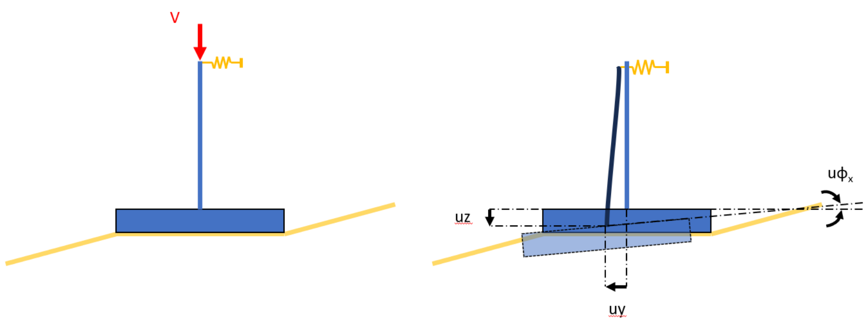

Figure 4.5: 2D Overview of load (F_z) and displacement $(uz,\ uy,\ u\phi_x)$ relation for a footing on a sloped seabed.

When considering the soil-structure interaction from a 2D perspective as in Figure 4.5, the footing on a slope during pure vertical loading (F_z) will cause a vertical displacement (u_z) along with horizontal (u_y) and rotational (u_{ϕ_x}). The direction of the horizontal displacement is inline with the downhill direction of the slope, which is the negative Y-axis in this specific case. The rotation of the footing will be in the direction of the slope itself, which is a rotation about the positive X-axis.
The soil constitutive model implemented is Hardening Soil which is determined based on a sand with relative density of 80% (RD80) [5].

The load-displacement in Z-direction is modelled for the complete preloading process for LP1 and LP2 in Appendix B. The loading-unloading behaviour of the RD80 model is highlighted with the unloading-reloading stiffness significantly larger than for virgin loading of soil.

In modelling the moment rotation curves about the X-axis, a positive (solid lines) and negative (dotted lines) direction are simulated to take the asymmetric seabed geometry into account. Interpreting

results for load-displacement in Y-direction Appendix B shows that when a load is applied in the positive direction, which aligns into the slope, the slope of the plots are higher than the plots in negative direction. Additionally, the plots in positive direction end at a higher value of F_y and for both directions, the higher the vertical load, the higher the plot ends. Both these findings show that for RD80, the stiffness (slope) and bearing capacity are higher with increasing vertical load and additionally when the footing is pressed into the slope.
When the moment-rotation around the X-axis is analysed, the negative direction has a higher stiffness (slope) than the positive. Additionally, there is a non-linear effect included in both directions which occurs earlier when vertical load is increased. For moment applied in negative direction, the non-linear effect occurs almost instantaneously when considering maximum vertical load, this effect can be explained by the soil failing locally, allowing hardening to occur where the stiffness decreases as the rotation increases.

When considering the load-displacement behaviour for LP2, the graph for Y-direction shows the same relation as with LP1, where with a decrease in vertical load, the initial stiffness and failure load decrease. However, the magnitude of the failure line is fairly symmetric showing that for decreased vertical load, the effect of the asymmetric seabed decreases.
When considering the moment-rotation about the X-axis, the results differ significantly for LP2 when compared to LP1. What is seen for LP2 is that with a decrease in vertical load, the stiffness increases (V-79.5) followed by a decrease (V-34).

4.4.2. Reaction loads and moments

Simulation using geotechnical model will give the reaction loads and moments due to seabed slope interaction occurring at the interface. A schematic overview of the model is given in Figure 4.6, where the reaction loads are measured at the interface (Node 5). The full results are tabulated below and used as an input for further structural modelling according to the framework as seen in Appendix B. Additionally the displacements of the leg-hull interface node and footing node are plotted for LP1 and LP2.

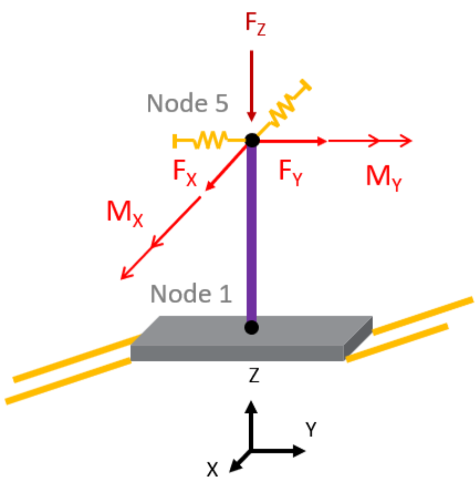

Figure 4.6: Overview of reaction loads at interface node (Node 5)

The reaction loads at the interface for LP1 show an overall increase with increase in vertical load, with M_y increasing most significant of all. This increase in M_y is out of place and not according to expectations on reaction loads that would occur in the current geometry. The expectation is that M_x and F_y will increase most significantly compared to M_y and F_x, which is not the case for the moments. This increase in moment is currently not able to be clarified but is expected to be due to assumptions on

soil-structure geometries. The variation of the soil-structure geometry is discussed in subsection 4.6.2. For LP2 there is little decrease in reaction loads at the interface, with an increase for F_x, M_y between steps 1 and 2 followed by a decrease between steps 2 and 3. However the moment M_x shows an increase with the decrease of vertical loads. This behaviour of loads not decreasing is due to the non-linear soil constitutive model where the soil is deformed introducing loads into the interface and upon unloading the soil medium remains deformed keeping loads present due to plasticity. However the clarification for the remaining loads that is given does not explain what causes the continued increase in M_x during unloading.
These results show that with the implementation of a full contact slope, the effects of a seabed slope are still captured. This effect is due to the unequal soil pressures originating from the asymmetric geometry. On the uphill direction of the slope, more bearing capacity is present compared to the downhill side due to less soil being present downhill. This unequal pressure causes an unequal pressure underneath the footing and an eccentric reaction force to occur, which causes rotation of the footing and thus a moment to occur.

The load-displacement of the footing and leg hull interface nodes are plotted in order to analyse the displacement of the leg during preloading and can be found in Appendix B. The load displacement plots will show the progression of the displacement and rotation of the selected nodes on the x-axis and the preload value on the y-axis.
The main take-away from the translation and rotation analysis during preloading at footing and leg hull interface nodes is that the translations of the system are in agreement with expectation but rotation is not. The rotation is expected to be large in the same direction as the slope (ϕ_x) due to the asymmetric seabed geometry, but this is not the case where the rotation of the footing is largest in the direction perpendicular to the slope (ϕ_y).
A cause of this phenomenon can be due to the application of the cantilever beams at the leg hull interface node in order to include interaction effects of the remaining structure into the geotechnical structure.

4.4.3. Foundation stiffness

For the first preloading cycle a given set of steps is taken and the foundation stiffness is determined using the geotechnical model using the methodology described in Figure 3.2 to calculate the non-linear stiffness at various steps in the preloading process. With the stiffness determined in each DOF in positive and negative direction, the values are then averaged in order to implement in a structural model as a set of uniaxial springs.
In this case, the steps taken are phases 1.1 and 1.2 for LP1 and 2.1 and 2.2 for LP2, modelling the first loading-unloading phase. Initially the resulting stiffness values for each DOF in both directions is given below before averaging is applied. Since the vertical foundation stiffness is only determined for downward direction ($K_{Z(-)}$), it will not be included in the following difference analysis. The full results of the foundation stiffness analysis can be found in Appendix B.
The results from implementing the prescribed framework shows that there is an unequal result for stiffness values in the same direction. This is due to the asymmetric seabed where the slope is is orientated uphill in positive Y-direction as can be seen in Figure 4.6.
In order to implement these values into a structural model as set of linear uniaxial springs, the positive and negative values are averaged an displayed in Appendix B for LP1 and Appendix B for LP2.

4.4.4. Reaction loads & foundation stiffness (full preload)

Here the full preload procedure with the loading and unloading of both LP's is modelled and the results being the reaction loads at the interface and foundation stiffness.
The key finding is the difference in the value for the final step, showing the path-dependent behaviour of the soil-structure interaction model. The difference is largest in horizontal direction (K_Y) at step 9 for both LP's, where the stiffness for LP2 is 8.08% larger than for LP1.
Another point of interest is that when unloading occurs for either LP, the horizontal foundation stiffness increase, which can be seen between steps 3 and 4 for LP1 in Appendix B and between steps 7 and 8 in LP2 in Appendix B. This phenomena needs further investigation an initial guess can be made that there is a correlation between the unloading-reloading behaviour of the soil constitutive model where

the E_{ur} is a factor 3 times larger than remaining stiffness moduli (E_{50} & E_{oed}) describing virgin loading conditions.

4.4.5. Comparison to industry standards

Here the industry standard values for foundation stiffness are compared to the averaged foundation stiffness values obtained from the proposed framework for a flat seabed and a sloped seabed. The result can be found Appendix B and Appendix B for flat seabed and in Appendix B and Appendix B for a sloped seabed.

Comparison to flat seabed case

When comparing the flat seabed foundation stiffness results to the industry standards, the main differences are in the order of magnitude between the results in horizontal (K_X and K_Y) and vertical (K_Z) translation stiffness values.
Firstly, looking at the horizontal translation stiffness values in X-direction (K_X) and Y-direction (K_Y) it can be observed that these values are significantly lower than the horizontal stiffness value calculated according to industry standard ($K_H = 2358.5\ MN/m$) where both cases are considered at maximum preload ($F_Z = 216\ MN$). This difference can be attributed to the fact that the currently selected geotechnical modelling method of SSFE does not allow for re-meshing between calculation steps. This assumption has as a consequence that the edges of the flat footing will never come into contact with the soil medium thus not allowing for any horizontal capacity to be built up during vertical loading. The horizontal stiffness is thus dependent purely on the capacity due to friction between the footing and soil.
Secondly, looking at the difference in magnitude for the vertical foundation stiffness values, the values for the flat seabed are significantly lower than industry standards at maximum preload ($F_Z = 216\,MN$). A cause here can be attributed to the fact that the standards are calculated using empirical relations based on an elastic perfect plastic soil constitutive model [3]. The values used to compare framework soil parameters and industry standard are the elastic stiffness moduli for HS (E_{oed}, E_{50}, E_{ur}) and Young's modulus (E). For the framework the elastic moduli determining behaviour due to shear and compression are E_{50} and E_{oed} respectively and are equal to $48\,MPa$ with elastic modulus for unloading and reloading $E_{ur} = 144\ MPa$.

Comparison to sloped seabed case

The main difference to consider in this case is the asymmetric response in horizontal foundation stiffness values in the framework results, while in industry standards, the lateral stiffness remains the same for X & Y directions. This is due to the asymmetry in the seabed geometry, where the slope runs from high to low parallel to Y-direction (K_Y). This effect of asymmetry of the seabed is also highlighted in the rotation about the X-axis ($K_{\phi,X}$) where the stiffness increases with vertical load at a quicker rate than for rotation about the Y-axis ($K_{\phi,Y}$).
Another point of consideration is the small difference in vertical foundation stiffness when comparing the flat and sloped cases calculated using the framework. The same can be said about the small difference in rotation stiffness values in X-direction ($K_{\phi,X}$). These small differences can be attributed to the assumption of soil-structure geometry where the footing is assumed in full contact with the flattened seabed as can be seen in Figure 3.1. In order to simulate the full effect of seabed slope, a different approach to simulating the soil-structure geometry must be taken, which is discussed in section 4.6.

4.5. Framework simulation

This section will discuss the results obtained from the combined geotechnical and structural modelling executed according to the methodology. The results are in the form of internal loads which correspond to the lower guide loads observed on JU's which are simulated to observe loads and moments introduced due to the presence of a sloped seabed.

4.5.1. Model Initialization

Inputs for beam properties can be obtained from modelling chapter 3.1, where all relevant beam properties are discussed. Creating the model gives the FE mesh which can be seen in Appendix B.

The model mesh is selected in such a way that the hull is described by single elements for starboard, port, forward, aft and diagonal directions. The legs on the other hand are meshed as 5 elements. The increase in amount of elements ensures an increase in calculation accuracy but at a cost of complexity and calculation time.
The next step is to identify the sloped seabed location and to cut the leg out of the FE mesh and simulate the leg during preloading process using geotechnical m for determining reaction loads. While for the remaining legs in the FE model, the foundation stiffness values are determined for a flat seabed which are then applied back into the structural model.

4.5.2. Load levels

Before the steps are applied according to the defined framework an analysis is implemented in order to describe the load levels occurring in the leg-hull interface values and can be found in Appendix B. These values can then be compared to the obtained leg-hull interface moments and loads in order to determine the magnitude of the sloped seabed interaction.

4.5.3. Single Slope

In order to determine the interaction effect of seabed slope, a loadcase must be defined which in this case refers to the location and orientation of seabed slope. The location and direction of the slope will dictate in which leg needs to be cut at the interface and simulated in soil-structure interaction model. In this load case, single slope refers to fact that there is only one leg orientated above a sloped seabed, as can be seen in Figure 4.7, where leg 1 is positioned on a slope.

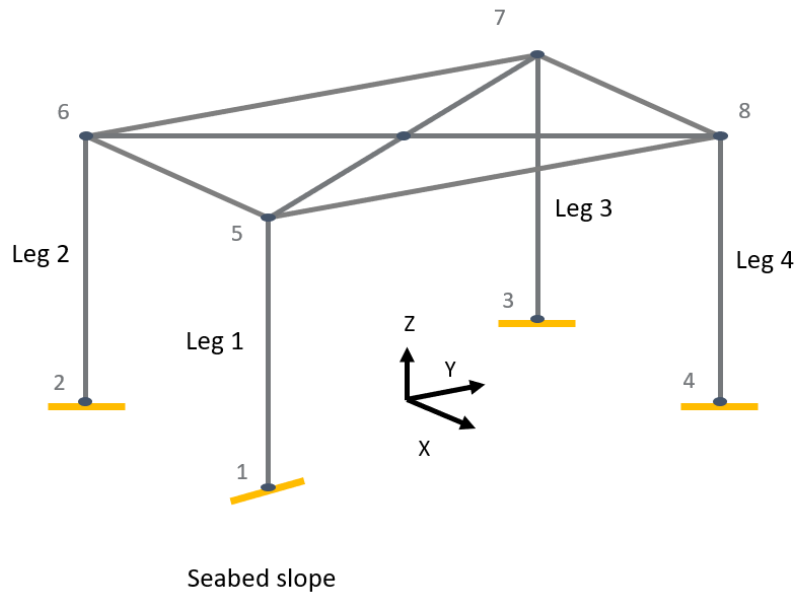

Figure 4.7: Load case where leg 1 is positioned on a sloped seabed with uphill direction in positive X-direction

The slope direction is aligned in the global Y-direction of the model as seen in Figure 4.7. For the following two loadcases, the load phases 1.1-1.2 and 2.1-2.2 will be modelled which translate to the first preloading phase. This is the phase where both LP2 start at equal vertical loads ($F_z = 125\ MN$) afterwards LP1 is set to full preload ($F_z = 216\ MN$) while LP2 is unloaded ($F_z = 34\ MN$).

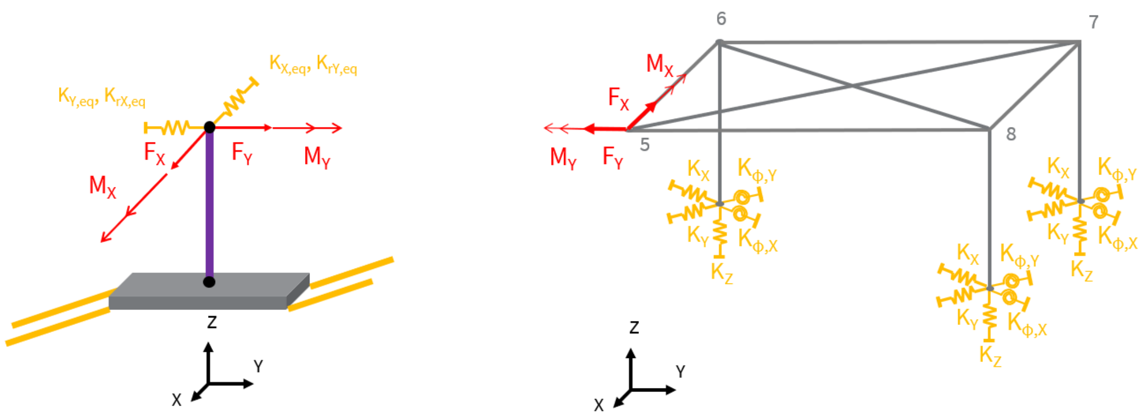

Figure 4.8: Overview of sloped leg transferring moment and force to JU

The figure above shows the equivalent geotechnical model for calculating reaction loads and moments (left) and equivalent structural model (right), which highlight the direction of seabed slope under leg 1 along with the direction of the reaction loads. Additionally the foundation stiffness values obtained through geotechnical modelling are also seen on the right of the image along with the equivalent hull stiffness at the interface node on the left model. The foundation stiffness values are used for a flat seabed which can be seen in Appendix B for LP1 (Leg 3) and Appendix B for LP2 (Leg 2 and 4). This plot highlights the integration between geotechnical and structural models in order to simulate seabed slope interaction effects in a JU during preloading.

Displacement plots

The simulation displayed will only contain 3 steps of the preloading process (V-125, V-170.5, V-216) as can be seen in Appendix B.
Here the displacement plot shows that the displacements of the interface node are in the same directions as the loads that are applied. Another observation is that there is no clearly visible bending of the hull (hull sagging) occurring, this is attributed to the large moment of inertia of the equivalent hull relative to the legs.

Moment plots

Simulating the moment occurring in the JU at each preload step to give an overview of load distribution as can be seen in Appendix B.
Here the moment plots show similar behaviour relative to each other, as the difference in input loads from geotechnical modelling remains relatively small. Another interesting point of attention is that there is a very small amount of load being transferred into the seabed relative to the amount of moment present in the leg-hull interfaces. This is mainly due to the relatively low rotation stiffness of the soil compared to the hull and legs.

4.5.4. Nodal results

The nodal results show the applied moments at the interface due to seabed slope interaction (node 5) and the moments at the remaining 3 leg-hull interface (nodes 6,7,8) and can be found in Appendix B. The moments are orientated along the global X- and Y-axes and colored red and blue respectively. Each figure consists of 2 plots with the left plot showing moment in global X-direction (red) and right plot the moment in global Y-direction (blue). The plots show the preload on the x-axis and the value for moment on the y-axis, with each step corresponding to an alphabetical letter, for the following cases only 3 steps are simulated, so only ”A”, ”B” and ”C” are shown.

The results start with the moment at node 5 which is equal to the reaction loads from the Plaxis3D model. What instantly jumps out in the results is that the moments at node 8 are largest in X-direction and moments at node 6 are largest in Y-direction. These results showing a magnitude larger than the input lead to the initial conclusion that horizontal loads at the interface will cause moments to occur at the remaining leg hull interface nodes (Nodes 6, 7 and 8).
Another result is the non-linear increase in moment at each step, which is due to the non-linear evolving reaction loads obtained from the previous section.

4.5.5. Nodal vertical load

These plots represent the vertical load occurring in the leg-hull interface nodes due to the seabed slope interaction and are found in Appendix B. The x-axis on these plots denote the step in the preloading process and the y-axis shows the internal vertical load at the interfaces. The interface for node 5 is equal to 0, as there is no vertical load transferred into the model from Model 1, so only the plots for the remaining leg hull interface nodes are shown (Nodes 6,7 and 8).

These plots show that there is a non-linear increasing vertical load present at each of the legs. The load at legs 2 and 3 are pointed downward while at leg 3 the load starts positive but flips during the preloading process. The vertical load at leg 4 is positive and has the largest magnitude.
When comparing the magnitude of the vertical reaction load (y-axis) to the input vertical preload used in the geotechnical model (x-axis), the vertical reaction load is significantly smaller than the input load. This result shows that for this framework with the assumption on soil-structure geometry, no significant vertical loads occur during the preloading procedure in the remaining legs.

4.5.6. Result analysis

Understanding the distribution of loads through the JU is relevant in order to recognize how the structure is affected by seabed interaction effects. This is analysed in the following subsection by individually applying loads and moments at the interface and measuring reaction loads at leg-hull interfaces and footing interfaces for the respective input load and or moment.

4.6. Sensitivity

One way to determine sensitivity of the framework is to identify important parameters for framework results. Identifying parameters are input parameters for the model and are selected based on variability and expected effect on global behaviour of framework developed. Some points of contention are listed as follows:

- Soil input parameters
- Soil-structure geometry

4.6.1. Varying soil input parameters

Here the soil parameters are reduced to observe effects of a weaker soil on soil-structure interaction. The soil parameters implemented are based on a soil with relative density of 80%, the parameters additionally selected are based on reduced relative density of 50% (RD50) and 25% (RD25). The methodology for these reduced soil parameters is kept the same while due to the decreased relative density, the soil strength and elasticity moduli decrease as can be seen in Table 3.4. For each of these soil cases the soil stiffness and reaction loads will be displayed for LP1 and LP2 which can be found in Appendix B

4.6.2. Varying soil-structure geometry

Another input parameter that can be adjusted in the framework is related to the combination of soil-structure geometry. This adjustment comes in the form of embedding the footing in a soil volume with weaker characteristics in order to indirectly have the footing in contact with the sloped seabed. This filling soil is selected as an MC soil constitutive model with a significantly lower elasticity modulus and the same strength parameters as the soil below which is kept at the previously selected HS soil constitutive model (RD80).

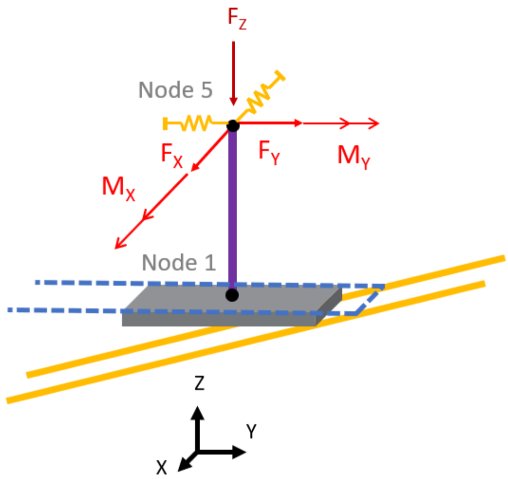

Figure 4.9: Overview of reaction loads at interface node (Node 5) - alternate soil-structure geometry

An overview of the suggested model is given in Figure 4.9 where the slope is only in contact with the edge of the footing, the latter of which is additionally embedded in a weaker soil. An overview from Plaxis3D highlighting the slope is given in Figure 4.10.

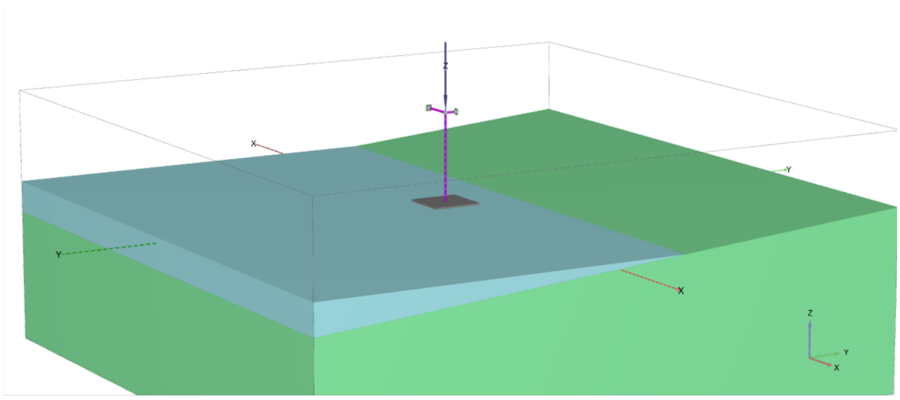

Figure 4.10: Overview of alternate soil-structure geometry

The soil constitutive model for the embedding soil is selected to include soil failure, as to ensure no tension in the soil will occur. As soil tension is possible in consolidated clayey types but not the case with frictional soils, where soil cohesion plays no role. Additionally, the embedding soil has the same strength parameters as the soil below (RD80) but reduced stiffness value as to ensure the soil displaces easily and spreads load through to stiffer sloped soil.

Table 4.5: Embedding soil parameters using MC soil constitutive model

γ_{unsat} $[kN/m^3]$	γ_{sat} $[kN/m^3]$	E $[kN/m^2]$	ν $[-]$	ϕ $[°]$	ψ $[°]$
18.2	20.3	480	0.3	38	8

With this variation for soil-structure geometry, the proposed framework can be applied in order to obtain vertical load-displacement behaviour along with reaction loads. The updated geometry will be implemented in the geotechnical model to determine reaction loads at interface. Before reaction loads are determined, the load displacement of the footing is simulated and compared to the original geometry case presented in Appendix B. These results can be found in Appendix B

Comparison original and alternate soil-structure geometries

Now that the results have been obtained for a various soil-structure geometries, it is important to highlight the differences between the two cases. The main differences can be classified as loads and displacements.

Starting off with the loads, the magnitude of the moment M_x shows the largest difference with an increase from original geometry ($M_x = 14\,MNm$) to alternate geometry ($M_x = -818\,MNm$) equating to an absolute 5842% increase in reaction moment. Additionally the magnitude of the moment in M_y in the original is of the same order of magnitude as M_x, which is not expected to occur, in the alternate geometry, this similar order of magnitude between the moments is not present. The order of magnitude for M_y is even smaller in the alternate geometry than in the original.

Moving on to displacements, the main difference is the displacement in the slope direction, where for the original geometry the footing displaces in a downhill direction while for the alternate geometry the footing displaces in an uphill direction. This is assumed to be caused by the increased rotation (ϕ_x) in the alternate case due to the more extreme slope.

Last note would be in the form of recommendation where the geotechnical modelling results need to be implemented into the structural model as specified in the framework in order to get the results from the full picture and compare load distribution behaviour.

4.7. Summary

To summarize, this chapter shows the results that are obtained from following the methodology and including model inputs and choices made in previous chapters. The results serve a goal in answering sub-questions described in section 1.2 in order to conclude the research by answering the main research question which is done in chapter 5.

The results for the first sub-question are related to non-linear soil-structure interaction in the form of reaction loads and moments during preloading (Model 1) and stiffness evolution during preloading (Model 2). Additionally, a validation is included in the form of soil-testing and comparison to industry standards. The main results from this section are that Plaxis 3D geotechnical simulation shows load-displacement results for the first loading-unloading phase in the preloading process for the most relevant directions (uz, uy and ϕ_x). These results show that for LP1 an increase in vertical load causes an increase in stiffness for all but in vertical direction, where a decrease is observed. Where for LP2 the same relation holds where with a decrease in vertical load, the stiffness will decrease in all directions but vertical. Additionally the result from Model 1 show the reaction loads at the interface of the leg during preloading which is in turn used as an input for structural modelling. While with Model 2, the foundation stiffness is determined for footing on a flat seabed.
To validate the geotechnical models, soil-testing is done in order to describe soil behaviour of various soil constitutive models. The main results for soil-testing are that the LE, MC and HS soil constitutive models range in complexity from low to high respectively but with each step in complexity, more accurate soil behaviour is achieved. The LE models the soil as a linear spring with infinite strength, while the MC and HS models include the non-linearity of soil failure using MC failure criterion. The MC model shows perfect plastic failure at the maximum effective stress while HS model shows an initial hardening (increase in slope) followed by decreased hardening (decrease in slope) up until the maximum effective stress is reached.
Another validation method are given by industry standards which give a range of stiffness values used in linear operation of footings on a seabed. These are used to compare obtained results with to ensure the order of the obtained stiffness values is within expected range and what the differences are between values.

The results of the second sub-question are related to describing a JU during a preloading operation. This is achieved by creating an equivalent model of the complex JU in order to capture the behaviour of a JU while reducing complexity. The equivalent model consists of 4 legs and a hull connected along the diagonals, to capture load-displacement behaviour of the JU, a finite element (FE) model is constructed. This FE model is then connected by a set of uniaxial springs at the footing node of the legs to simulate soil-structure interaction.

The results of the third sub-question focus around combining the geotechnical with structural domain which is achieved by combining the results of the non-linear soil-structure interaction model into a structural finite element model of an equivalent JU. This is done by simulating one leg of the structural FE model on a slope in the geotechnical model, while the remaining footings apply a foundation stiffness determined with the same geotechnical model but for solely the footing. The results come in the form of displacement and moment plots which are analysed in order to give insight into the distribution of loads in the JU for various stages in the preloading process. The current model shows that the applied moments due to sloped seabed interaction are captured by a set of vertical load couples in the legs. While the horizontal loads cause moments to occur in leg-hull interfaces in X- and Y-directions and a vertical load couple in the legs. The effects of the horizontal input load due to seabed interaction is significantly larger than for moment input due to seabed interaction. However with the current assumptions made for soil-structure geometry, the magnitude of the loads occurring in the JU are found to be significantly lower than expected load levels.

The final sub-question is related to the sensitivity of the proposed framework, which is done firstly by comparing 3 different soils based on relative density which in turn determine soil strength and soil stiffness moduli. The relative density is 25, 50 and 80 % and show that with a decrease in relative density, the stiffness decreases allowing for increased displacement of the footing. The second method for determining framework sensitivity is done by introducing an alternative method for modelling soil-structure geometry. This method is executed by embedding the footing in a soil with significantly less stiffness in order to ensure addition of nodes between soil and structure, indirectly connecting the structure to seabed. The results of the alternative geometry show a magnitude of reaction moments at leg-hull interface which are in range of the expected load levels.

5 Conclusion

This chapter formulates a concise summary of the research presented in the paper, starting with reviewing the main research question. Afterwards some key findings are highlighted followed by a closing statement. The main research question is stated as follows:

How does the presence of a sloped seabed influence a four legged jack-up during preloading operation?

In order to answer this main research question, a set of sub questions are proposed to divide the process into manageable pieces. The following 4 paragraphs will each state the sub question and give an answer to the question.

first sub question tackles geotechnical modelling for a footing on a sloped seabed and is stated as:*How will the presence of a sloped seabed affect the footing response during preloading?*. In order to answer this question, soil-structure interaction for a footing on a sloped seabed is simulated using Plaxis3D. As Plaxis3D is a small strain finite element program which does not allow for re-meshing an assumption is made where the bottom of the footing is in full contact with the seabed as to allow for stable numerical calculations. Additionally the geometry of the leg and a set of stiffness values representing the hull of the vessel are added to the model. With the geometry implemented, the preloading process can be simulated as a set of discrete steps selected of the continuous preloading process in order to determine reaction loads and foundation stiffness values at critical points during the process. Implementing this geotechnical model the soil-structure interaction shows loads and moments occurring due to seabed slope effect and the footing rotating to align with the slope and the footing displacing downhill.

The second sub question envelops the structural modelling required to simulate a JU and is stated as: *How can a structural model be implemented to describe a JU during preloading?*. Describing a JU during preloading is achieved by implementing an equivalent finite element model using parameters representative of the leg and hull of a NG-20000X. The legs and hull are divided into nodes and elements with the hull including two diagonal elements, creating diagonal leg pairs (LP1 and LP2). The mesh is then solved using finite element modelling implemented using an in-house GustoMSC finite element solver.

The third sub question describes the combination of the geotechnical and structural models in a framework as is noted as: *How can a framework combining geotechnical and structural domains be employed to obtain loads in a jacking system of a JU during preloading?*. Answering this sub question is done by defining the calculation steps in an overview showing the interaction between geotechnical and structural models. In the current framework one leg is assigned to be on a seabed slope which is then taken cut out of the 4 legged structural JU model and simulated using the Plaxis model. The location where the model is cut is referred to as the interface and in order to include hull stiffness effects in the Plaxis model, the equivalent stiffness of the hull is calculated for the 3 legged JU and implemented at the interface node in the geotechnical model. With this model complete the preloading process can be simulated for discrete steps obtaining the reaction loads & moments and foundation stiffness values. Adding the results into the structural FE model, the system can be solved in order to determine the loads occurring in the JU due to sloped seabed interaction. The results from the model show that the foundation stiffness is relatively low compared to the structure as a very small amount of the moment is taken by the soil but as a vertical load couple in the legs. On the other hand the horizontal loads at the interface cause horizontal reaction loads to occur at the remaining 3 footings, which in turn cause a reaction moment to develop at each of the leg-hull interface nodes above the respective footing node.

The final sub question takes a look at the sensitivity of the model by varying the input and certain assumptions to show behaviour of the framework and is defined as: *How does the sensitivity of the model vary with changes in input parameters?*. There are two cases taken into consideration for sensitivity; a variation of soil parameters and a variation on soil-structure geometry. The former is implemented to show variation of reaction loads & moments and foundation stiffness values. The latter variation is implemented as the reaction loads & moments due to the full contact footing on the sloped seabed are relatively small to calculated load levels.This alternate geometry is executed by implementing a full slope and a weaker embedding soil in order to allow the nodes of the footing to indirectly make contact with the sloped seabed. The results of the variation show reaction moments of the same order of magnitude as the calculated load levels.

One key finding made in this research is the framework which allows for soil-structure interaction on a sloped seabed to be combined with a structural finite element model. This is significant as in current literature there is very little to find on soil-structure interaction on sloped seabeds for 4 legged JU's. There is research done in comparable cases where the soil-structure interaction for spudcan penetration on footprints are analyzed for single spudcans [10] or 3 legged JU's [15]. There is also research done for 4 legged JU's during preloading but with a focus on time-dependent soil response (consolidation) for active preloading [28].
Another key finding is that during preloading operations, the largest internal moment occurring in the jacking systems are not present along the actively preloading LP but in the unloading LP. The largest moment in X-direction occurs at Leg 4 while in Y-direction the largest moment occurs at Leg 2, when considering the first preload cycle. This is relevant in the context of real-life operations where a large load occurring on a jacking system of a leg could be due to the seabed slope of another leg, along the opposite diagonal.
Additional finding shows that moment is distributed through the JU as a vertical load couple, which can influence the amount of vertical load on the remaining legs, potentially causing lower vertical loads at the footings. This can be an unfortunate effect as during preloading the soil under a spudcan must be mobilized in order to ensure foundation capacity during further operation of the vessel. However in the current framework, the relative vertical load induced in the legs is low. Another effect that needs to be taken into account is the added moment due to the sloped seabed, although with the current framework this effect remains small, however with the alternative geometry implemented in the sensitivity chapter the magnitude of all loads and effects are increased. This increase in moment can have a negative effect on the structural integrity of the JU and bring the safety of the JU in problems.

Finally reviewing the big picture, the answer to the main research question is given by creating a framework which combines 2 geotechnical and a structural model in order to determine leg-hull interface loads caused by the presence of a sloped seabed. The effect of seabed slope is shown to increase load which can in turn have a negative effect on the structural integrity of a JU, potentially leading to failure and unsafe operation.

6
Discussion & Recommendations

This chapter is dedicated to discussing the obtained results along with assumptions made during the research and giving recommendation on continuation of research on this subject.

6.1. Discussion

The first point of discussion arises when considering the selection for seabed slope and shape of structure of a flat footing. As stated before this is chosen in order to ensure full contact between the mesh of the soil and structure as a SSFE model is implemented, which does not allow for re-meshing. As shown in results for soil-structure modelling, the proposed geometry set-up does show behaviour according to predicted direction but the magnitude of the reaction forces is expected lower than in reality would occur. This is due to the large eccentricity of reaction load which is present when penetrating a sloped seabed caused by the area of the structure in contact with the seabed being eccentric. An attempt to simulate the geometric eccentricity is done in sensitivity by placing the footing above the sloped seabed and adding an additional soil layer between footing and seabed. This is done to work around the non re-meshing behaviour of Plaxis 3D. These results lead to higher moments occurring during preloading in order of magnitude of expected load levels.
The second point of discussion relates to the choice for an uncoupled assumption for foundation stiffness in the soil-structure interaction model. In reality there is coupling between DOF's which are not taken into account in the current model. The inclusion of coupling would increase the accuracy but also complexity. The current methodology applies a test load and moment in uniaxial directions to obtain the uncoupled stiffness, but to implement the coupled stiffness values, a combined loading must be applied as a test phase and the coupled stiffness values could be determined. This combined test phase must be applied for all combinations of DOF's to create a fully populated stiffness matrix which can then be implemented into a structural model.
The third point of discussion is the assumption of a static model for simulating a JU during preloading, by removing any time-dependent terms (acceleration & velocity) from the PDE's when setting up the structural model. This is assumed as the preloading process is a slow process which is only performed under favourable weather conditions thus neglecting environmental loads such as wind and wave loads. In reality however these environmental loads, however small may introduce base shear and a moment on the system when the legs make contact with the seabed. This interaction will lead to a variation in soil-structure interaction and combined with a slope could lead to significant footing displacements, introducing large loads into the JU.
The fourth point of discussion is the connection between the structural model and geotechnical m, where an equivalent value is chosen based on a load-displacement analysis. In this load-displacement analysis model the values for foundation stiffness are assumed as a constant value, but as is seen in this report, the foundation stiffness is path dependent. In order to determine the effect of a varying equivalent stiffness, a range of stiffness values must be implemented in order to determine how the updated stiffness will affect the load distribution in the geotechnical model when determining reaction loads. This variation in equivalent stiffness will have a large effect as the equivalent stiffness values

are relatively large when compared to the previously calculated foundation stiffness values.

6.2. Recommendations

With the proposed methodology valuable insight is given to the soil-structure interaction for a footing on a sloped seabed and the combining of geotechnical and structural modelling domains, but still topics for further research recommendations are identified. The recommendations can be divided in 3 main categories; soil-structure, structural and general recommendation for future studies based on the executed research.

6.2.1. Soil-structure related recommendations

One main recommendation for future implementations is based around the choice of soil modelling method, this research uses a small-strain modelling method which does not allow for re-meshing between calculations steps. But inherently a penetration calculation should allow for re-meshing especially when a spudcan shape is to be introduced where with increased penetration, more area of the footing comes in contact with the seabed causing an increase in bearing capacity. This leads to the recommendation of implementing a LDFE model as re-meshing is allowed by implementing a combination of finite element methods. The use of LDFE would predict a much more accurate load-displacement behaviour with a cost of complexity and time.

A second recommendation is the addition of seabed slopes and spudcan shaped in order to determine more accurately the effect of shape and slope on reaction loads and moments along with stiffness values. The spudcan shape can be incorporated by importing a spudcan file into Plaxis3D and embedded into the soil. This embedment must be done with care as foundation resistance is a function of depth and with a drained soil with a relatively high friction angle, the penetration is low, so a realistic value for embedment must be chosen.

A third recommendation is given for the mesh refinement of the soil continuum, as a value for mesh coarseness has been selected as 0.03. But in order to validate the mesh coarseness, a mesh refinement should be implemented for various coarseness values to confirm convergence of the models. This can be implemented by creating a local mesh refinement around the structure as most strain will occur due to soil-structure interaction. Per iteration of coarseness value, the reaction loads can be compared in order to ensure convergence of the results to a single value.

A fourth recommendation comes in varying the equivalent stiffness value in the geotechnical model as the ratio of stiffness between cantilever beams and foundation stiffness affects the load distribution. An increase in equivalent stiffness will lead to a larger reaction load and smaller displacement and rotation at the interface node.

6.2.2. Structural related recommendations

The current structural model is made on the basis of an equivalent JU, where the 3D X-braced legs are represented by means of a stick model and hull modelled as single beam elements with a rigid connection to the legs. To include more realistic JU behaviour, the recommendation is to increase complexity of equivalent model by increasing nodes describing the legs of the JU along with the hull.

Another recommendation comes when considering the mesh of the hull and 4 legs consists of only 21 nodes and is to refine the mesh especially when considering the large loads to ensure the results of the model converge. This is useful as this refinement acts as a validation of the structural result.

6.2.3. General recommendations

One recommendation for expanding on the current sensitivity study is to include a larger variation of sand types for the HS soil input in order to separate effects of soil strength parameters and soil elasticity parameters. As with the current sensitivity, the relative density is varies, which has a set linear relation with soil strength and elastic moduli based on empirical formulations. These soil parameters can be obtained through literature findings or by means of obtaining a soil sample and conducting tri-axial and oedometer test to determine soil strength and elastic moduli.

Another recommendation arises when considering the choice of this research to focus on preloading of a JU while other operational cases are also affected by a sloped seabed. One such operational case that should be looked into further is the jacking to preload airgap which occurs before the preloading process. The jacking phase has been side-stepped due to the preload phase inducing larger leg loads which are expected to in turn cause larger reaction loads when considering soil-structure interaction. To fully understand the preloading process of a JU, the jacking process which occurs before preloading should also be taken into consideration.

References

[1] Bienen B. and Cassidy M.J. “Three-Dimensional Dynamic Analysis of Jack-Up Structures”. In: *Advances in Structural Engineering* (2006), pp. 19–37.

[2] GustoMSC Resources B.V. *Measurement system, leg guide, Jack-up platform*. Mar. 2019.

[3] R. Bell. “The analysis of offshore foundations subjected to combined loading”. In: (1991).

[4] M.D. Bolton. *A guide to Soil Mechanics*. 1991.

[5] R.B.J Brinkgreve, H.K. Engin, and E Engin. “Validation of empirical formulas to derive model parameters for sands”. In: 2010, pp. 137–142. ISBN: 9780415592390. DOI: 10.1201/b10551-25.

[6] R.B.J. Brinkgreve. *PLAXIS Material Models Manual*. 2024. URL: https://bentleysystems.service-now.com/$viewer.do?sysparm_stack=no&sysparm_sys_id=c3ba7d7347c6ca5888c56642846d43be.

[7] M.J. Cassidy. “Non-Linear Analysis of Jack-Up Structures Subjected to Random Waves”. In: (1999).

[8] M.J. Cassidy, C.M. Martin, and G.T. Houlsby. “Development and application of force resultant models describing jack-up foundation behaviour”. In: *Marine Structures* 17 (3-4 May 2004), pp. 165–193. ISSN: 09518339. DOI: 10.1016/j.marstruc.2004.08.002.

[9] *Offshore soil mechanics and geotechnical engineering*. Standard. Der Norske Veritas, Sept. 2021.

[10] C.T. Gan, C.F. Leung, and Y.K. Chow. “A study on spudcan footprint interaction”. In: IHS/BRE Press, 2008, pp. 861–872. ISBN: 9781848060449.

[11] G. Gottardi, G.T. Houlsby, and R. Butterfield. “Plastic response of circular footings on sand under general planar loading”. In: *Geotechnique* 49 (4 1999), pp. 453–469. ISSN: 00168505. DOI: 10.1680/geot.1999.49.4.453.

[12] J.B. Hansen. “A revised and extended formula for bearing capacity”. In: (1970).

[13] M. Hossain and M. Randolph. “Bearing behaviour of shallow foundations on clays - offshore and onshore, research and practice”. In: *Proceedings of the 17th International Conference on Soil Mechanics and Geotechnical Engineering*. Vol. 1. 2009, pp. 570–573. ISBN: 9781607500315.

[14] G. Houlsby and C. Martin. “Undrained bearing capacity factors for conical footings on clay”. In: *Geotechnique* (2003), pp. 513–520.

[15] M. J. Jun et al. “Global jack-up rig behaviour next to a footprint”. In: *Marine Structures* 64 (Mar. 2019), pp. 421–441. ISSN: 09518339. DOI: 10.1016/j.marstruc.2018.12.002.

[16] D. R. Karukola. *Chronological development of offshore platforms*. 2017. URL: https://www.researchgate.net/publication/331382546.

[17] M. G. Korzani and A. A. Aghakouchak. “Soil-structure interaction analysis of jack-up platforms subjected to monochrome and irregular waves”. In: *China Ocean Engineering* 29 (1 Mar. 2015), pp. 65–80. ISSN: 21918945. DOI: 10.1007/s13344-015-0005-3.

[18] *MPI Resolution stretches legs*. 2016. URL: https://renews.biz/40253/mpi-resolution-stretches-legs/.

[19] *NG-20000X Self-propelled jack-up*. 2024. URL: https://www.nov.com/products/ng-20000x-self-propelled-jack-up.

[20] *NOV to design and equip Havfram’s first wind installation jack-up vessel*. 2022. URL: https://www.nov.com/about/news/nov-to-design-and-equip-havframs-first-wind-installation-jack-up-vessel.

[21] *Petroleum and natural gas industries — Site-specific assessment of mobile offshore units —Part 1: Jack-ups*. Tech. rep. INternational Organisation for Standardisation, 2016.

[22] F. Pisanò, L. Flessati, and C. Di Prisco. “A macroelement framework for shallow foundations including changes in configuration”. In: *Geotechnique* 66 (11 Nov. 2016), pp. 910–926. ISSN: 17517656. DOI: 10.1680/jgeot.16.P.014.

[23] M. Randolph and S. Gouvernec. *Offshore geotechnical Engineering*. Spon Press, 2011. ISBN: 978-0-203-88909-1.

[24] J. Reddy. *Introduction to the Finite Element Method*. Ed. by J Holman and J Lloyd. Second Edition. McGraw-Hill, Inc, 1993. ISBN: 0-07-051355-4.

[25] K.H. Roscoe, A.N. Schofield, and C.P. Wroth. *On the yielding of soils*. 1958. DOI: 10.1680/geot.1958.8.1.22.

[26] A.N. Schofield and P. Wroth. *Critical State Soil Mechanics*. 1968. ISBN: 9780641940484.

[27] Y Shin et al. “Spudcan Penetration Behaviour on a Sloping Seabed by Numerical Analysis and Centrifuge Modeling”. In: 2021. URL: https://www.researchgate.net/publication/350631298.

[28] W. Sonnema et al. “Preloading of four-legged jack-ups in clay: Geotechnical time effects and fulfilment of preloading criteria”. In: *Ocean Engineering* 278 (2023). ISSN: 00298018. DOI: 10.1016/j.oceaneng.2023.114425.

[29] R. W.P. Stonor et al. “Recovery of an elevated jack-up with leg bracing member damage”. In: *Marine Structures* 17 (3-4 May 2004), pp. 325–351. ISSN: 09518339. DOI: 10.1016/j.marstruc.2004.08.007.

[30] K. Terzaghi. *Theoretical Soil Mechanics*. John Wiley Sons, Ltd, 1943. ISBN: 9780470172766. DOI: https://doi.org/10.1002/9780470172766.ch2.

[31] N.I. Thusyanthan. “Seabed Soil Classification, Soil Behaviour, and Pipeline Design”. In: Society of Petroleum Engineers (SPE), Apr. 2012. DOI: 10.4043/23297-ms.

[32] Ali Tolooiyan, Kenneth Gavin, and Ashley P. Dyson. “Estimation of spudcan penetration in variable sand deposits with the Arbitrary Lagrangian Eulerian Finite Element Method”. In: *Ocean Engineering* 281 (Aug. 2023). ISSN: 00298018. DOI: 10.1016/j.oceaneng.2023.114955.

[33] Dong Wang et al. *Large deformation finite element analyses in geotechnical engineering*. Apr. 2015. DOI: 10.1016/j.compgeo.2014.12.005.

[34] Zhang et al. “Jack-up spudcan penetration analysis: Review of semi-analytical and numerical methods”. In: CRC Press/Balkema, 2015, pp. 1341–1346. ISBN: 9781138028487. DOI: 10.1201/b18442-204.

[35] Yi kan Zheng, Shi lian Zhang, and Lei Lai. “Load distribution on the hull-leg connection components of a jack-up”. In: *Journal of Shanghai Jiaotong University (Science)* 20 (6 Dec. 2015), pp. 721–728. ISSN: 19958188. DOI: 10.1007/s12204-015-1682-z.

A

Empirical formulas to derive Hardening Soil model parameters

This chapter gives all empirical formulas used to obtain model parameters for soil constitutive model in Plaxis. The specific soil constitutive model implemented is Hardening Soil, which is a non-linear soil constitutive model which is able to model shear and compression hardening.
The empirical formulas have been created in order to implement complex soil models when limited geotechnical data is available for a given project. As the scope of this research does not include testing of soil samples, this set of empirical formulas will be implemented.
These empirical formulas take only relative density of a sand as an input, which can be calculate using void ratios.

$$RD = \frac{e_{max} - e}{e_{max} - e_{min}} \tag{A.1}$$

With e as the current void ratio, e_{max} is the maximum void ratio (loosest packing), and e_{min} the minimum void ratio (densest packing). The relative density can be seen as a percentage of filled void ratio, the unit is therefore percentage [%]. Before diving into empirical formulations, the relative densities can be implemented to obtain unit weights.

$$\gamma_{unsat} = 15 + 4.0RD/100 \tag{A.2}$$

$$\gamma_{sat} = 19 + 1.6RD/100 \tag{A.3}$$

These unit weights are given in kN/m^3 and give the unit weights for two cases; when the soil is saturated with water and without water saturation.
The stiffness parameters needed for the HS model are calculated as a reference stiffness which is calculated with a reference stress level ($p_{ref} = 100kN/m^2$). This is a pointer to the stress dependent stiffness property of the HS model, for which the rate of stress dependency is determined by m. The stiffness parameters are the secant stiffness at 50% of the failure stress (E_{50}), the oedometer stiffness (E_{oed}) and the loading-unloading stiffness (E_{ur}).

$$E_{50}^{ref} = 60000RD/100 \tag{A.4}$$

$$E_{oed}^{ref} = 60000RD/100 \tag{A.5}$$

$$E_{ur}^{ref} = 180000RD/100 \tag{A.6}$$

$$m = 0.7 - RD/320 \tag{A.7}$$

The strength parameters of the soil model are given with internal angle of friction (ϕ) and dilation angle (ψ).

$$\phi = 28 + 12.5RD/100 \tag{A.8}$$

$$\psi = -2 + 12.5RD/100 \tag{A.9}$$

These empirical formulas give way to use HS soil model with limited geotechnical input.

B

Confidentiality annex

This section has been removed as it contains confidential information and results provided by collaborative research partner GustoMSC.